EIC Detector R&D Progress Report

Project ID: eRD14

Project Name: PID Consortium for an integrated program for Particle Identification (PID) at a future Electron-Ion Collider

Period Reported: from 7/1/2018 to 12/31/2018

Contact Persons: Pawel Nadel-Turonski and Yordanka Ilieva

Project Members:

M. Alfred[10], B. Azmoun[3], F. Barbosa[15], W. Brooks[20], T. Cao[24], M. Chiu[3], E. Cisbani[13,14], M. Contalbrigo[12], S. Danagoulian[17], A. Datta[23], A. Deldotto[13], M. Demarteau[2], A. Denisov[11], J.M. Durham[16], A. Durum[11], R. Dzhygadlo[9], D. Fields[23], Y. Furletova[15], C. Gleason[24], M. Grosse-Perdekamp[22], J. Harris[25], M. Hattawy[18], X. He[8], H. van Hecke[16], T. Horn[4], J. Huang[3], C. Hyde[18], Y. Ilieva[24], G. Kalicy[4], A. Kebede[17], B. Kim[5], E. Kistenev[3], M. Liu[16], R. Majka[25], J. McKisson[15], R. Mendez[20], I. Mostafanezhad[21], P. Nadel-Turonski[19], K. Peters[9], W. Roh[8], R. Pisani[3], P. Rossi[15], M. Sarsour[8], C. Schwarz[9], J. Schwiening[9], C.L. da Silva[16], N. Smirnov[25], J. Stevens[6], A. Sukhanov[3], X. Sun[8], S. Syed[8], R. Towell[1], G. Varner[21], R. Wagner[2], C. Woody[3], C.-P. Wong[8], J. Xie[2], Z.W. Zhao[7], B. Zihlmann[15], C. Zorn[15].

[1] Abilene Christian University, Abilene, TX 79601
[2] Argonne National Lab, Argonne, IL 60439
[3] Brookhaven National Lab, Upton, NY 11973
[4] Catholic University of America, Washington, DC 20064
[5] City College of New York, New York, NY 10031
[6] College of William & Mary, Williamsburg, VA 2318
[7] Duke University, Durham, NC 27708
[8] Georgia State University, Atlanta, GA 30303
[9] GSI Helmholtzzentrum für Schwerionenforschung, 64291 Darmstadt, Germany
[10] Howard University, Washington, DC 20059
[11] Institute for High Energy Physics, Protvino, Russia
[12] INFN, Sezione di Ferrara, 44100 Ferrara, Italy
[13] INFN, Sezione di Roma, 00185 Rome, Italy
[14] Istituto Superiore di Sanità, 00161 Rome, Italy
[15] Jefferson Lab, Newport News, VA 23606
[16] Los Alamos National Lab, Los Alamos, NM 87545
[17] North Carolina A&T State University, Greensboro, NC 27411
[18] Old Dominion University, Norfolk, VA 23529
[19] Stony Brook University, Stony Brook, NY 11794
[20] Universidad Técnica Federico Santa María, Valparaíso, Chile
[21] University of Hawaii, Honolulu, HI 96822
[22] University of Illinois, Urbana-Champaign, IL 61801
[23] University of New Mexico, Albuquerque, NM 87131
[24] University of South Carolina, Columbia, SC 29208
[25] Yale University, New Haven, CT 06520

Abstract

Excellent particle identification (PID) is an essential requirement for a future Electron-Ion Collider (EIC) detector. Identification of the hadrons in the final state is critical to study how different quark flavors contribute to nucleon properties. Reliable identification of the scattered electron is important for covering kinematics where pion backgrounds are large. The EIC PID consortium (eRD14) was formed to develop an integrated PID program using a suite of complementary technologies covering different ranges in rapidity and momentum, as required by the asymmetric nature of the collisions at the EIC. The PID consortium has also worked closely with BNL and JLab to ensure that the specific R&D projects are compatible with the detector concepts that are being pursued there.

Table of Contents

1. Introduction

Identification of hadrons in the final state is essential for key EIC measurements formulated in the EIC White Paper and referenced in the NSAC Long Range Plan. These include 3D imaging of the nucleon in momentum space through semi-inclusive DIS (where flavor tagging can tell us about the transverse momentum distributions and, potentially, the orbital angular momentum of the strange sea), and open charm (with decays of D-mesons into kaons), which is important for probing the distribution of gluons in protons and nuclei.

Satisfying the PID requirements within the very asymmetric kinematics of the EIC (discussed in detail in the eRD14 proposal for FY19) requires a suite of detector technologies that can address the specific challenges (in terms of momentum coverage, available space, *etc.*) encountered in various ranges of rapidity. Thus, the integrated PID program pursued by the eRD14 Consortium includes different detector systems for each endcap and the central barrel, as well as corresponding sensor and readout solutions. While we ensure compatibility with the detector concepts developed at BNL and JLab, all funded R&D being pursued by the consortium is conceptually novel. The dual-radiator RICH (dRICH) for the hadron endcap is the first such design for a solenoid-based collider detector. The modular aerogel RICH (mRICH), primarily intended for the electron endcap, introduces lens-based focusing, which improves momentum coverage and reduces the required sensor area. The compact, high-performance DIRC for the barrel combines new optics for spatial imaging with good timing (<100 ps rms) to allow a significant improvement in momentum coverage compared with the state-of-the-art. The funded work on photosensors in high magnetic fields and on adaptation of LAPPDs to EIC requirements is also aimed at developing a new generation of devices. Starting in FY18, the sensor effort has been extended to include corresponding readout electronics.

In order to be able to coherently evolve one integrated concept, the key consortium goals for FY19 were start moving the dRICH from simulation only to initial prototyping (for instance to study the gas-aerogel interface); to analyze the data from the 2nd mRICH test beam in 2018, and to evaluate radiation-hard lens solutions for the DIRC (as well as carrying out one more test beam at CERN). The high-B photosensor and LAPPD efforts have continued, and the new readout-electronics activities led by the Hawaii group and INFN are on track to deliver a first set of devices for the mRICH test beam at Fermilab in the early summer of 2018. The targeted effort on electronics development for the high-resolution TOF was completed in FY18, and no funds were requested in FY19.

The consortium has also been closely following the issue of what appeared to be unused funds, which turned out to largely be an artifact of the administrative procedures used (there were no actual unspent dollars). To avoid future misunderstandings, we will keep monitoring the expenditures so that we always can provide the program manager and the committee with up-to-date information.

2. Hadron Identification Detectors

2.1 Summary

The funded R&D on the three Cherenkov systems has been proceeding very well, and they all promise significant advances over the fallback options (single-radiator gas RICH for the dRICH, proximity-focusing aerogel RICH for the mRICH, or a DIRC geared only towards spatial imaging or timing). There was no FY19 funding request for mRPC-based high-resolution TOF.

2.2 Dual-Radiator RICH (dRICH)

The dual Ring Imaging Cherenkov (dRICH) detector is intended to provide full hadron identification (π/K/p separation of better than 3 sigma) from ~3 GeV/*c* to ~50 GeV/*c* and electron identification (e/π separation) up to about 15 GeV/*c*, in the ion-side end-cap of the EIC detector, covering angles up to 25°.

2.2.1 Past

2.2.1.1 What was planned for this period?

The main goals for the second half of 2018 were a first refinement of the prototype design and the consolidation of the event-based reconstruction algorithm implemented in the first half of the year. Within an initiative by a number of Italian researchers interested in the EIC project, efforts were also spent to submit a co-funding request for the dRICH future prototyping activities to the Nuclear Physics Commission of the Italian National Institute of Nuclear Physics (INFN). Some of the planned prototyping activities are shared with the mRICH development.

2.2.1.2 What was achieved?

The baseline performances achieved in the first half of 2018 with a realistic Geant4/GEMC model and related simulations was further consolidated, including the originally implemented track-based algorithm for Cherenkov angle reconstruction, and extended to an event-based reconstruction to properly handle events with multiplicity larger than 1. Figure 2.2.1 shows the latest identification performances obtained by the latter method, in SIDIS-like physics experiment conditions.

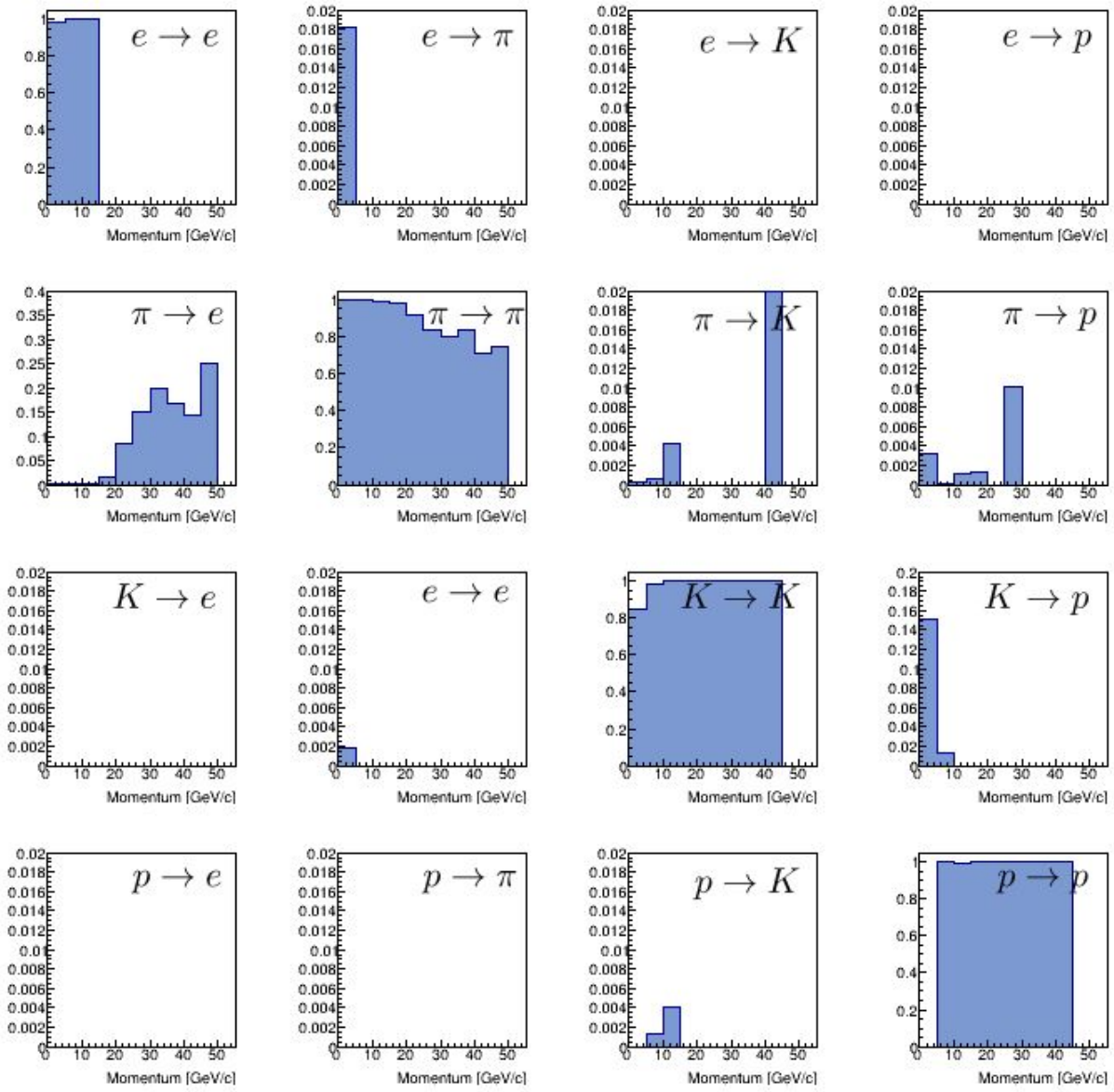

Figure 2.2.1: Particle identification performances in relative particle populations typical of a SIDIS experiment. The values on the Y axis, together with the label *A*→*B* within each plot, show the probability that particles of type *A* are identified as particles of type *B*. For example, the probability that true electrons are identified as electrons is mostly 100% (top right plot). Note that the hadron identification is excellent up to about 50 MeV/*c* (where statistics is small). The *e*/π identification can be improved by combining information from other detectors.

The main result of this detailed analysis confirms the design goals (Table 2.2.1). However, some of the adopted/proposed solutions do require detailed experimental studies.

	Nominal Momentum Threshold [GeV/*c*]	
Particle	Aerogel (n=1.02)	Gas (C2F6, n=1.0008)
Electron	0.003	0.013
Pion	0.69	3.49
Kaon	2.46	12.3
Proton	4.67	23.5

Table 2.2.1: Momentum threshold for each particle in the considered radiators; (refractive indices are evaluated at about 300 nm wavelength).

The main results of the dRICH studies have been presented at the RICH2018 conference.

The software codes have been documented and arranged in an easy-to-transfer way, taking into account the transition phase due to the end of Alessio Del Dotto's postdoctoral fellowship (May 2018).

The key components proposed for the dRICH baseline have been critically analyzed for the definition of the dRICH prototype. The aerogel performance, its long term stability and interplay with gas(es) need to be properly and carefully evaluated in an experiment in order to avoid the problem faced by the LHCb experiment, in particular given the very limited choices of aerogel providers; these may require repeated and extended basic measurements. The C_2F_6 fluorocarbon is the golden candidate as a gas radiator. Literature data on fluorocarbons are relatively poor. In the most up-to-date studies of C_2F_6 [Hor17, Chr99], the number of Cherenkov photons is extrapolated from the existing, more copious, CF_4 data, by scaling the refractive indexes. Also, the scintillation photon yield in the gas radiator may represent a limitation. This, and the realistic number of Cherenkov photons need to be investigated. Such studies can be beneficial also for the gas RICH in the BNL spectrometer. Lastly, if the measured performance of the C_2F_6 is found to be inadequate, different alternatives (***e.g.*** C_2F_6 gas mixture or a completely different gas mixture with similar refractive index) need to be investigated and tested.

Photon detector: SiPMs represent a potential readout solution for the dRICH, due to their magnetic-field immunity, compact design, and sensitivity to single photons. As, at present, they need to be adequately cooled and thermally stabilized, the best trade off between complexity and effectiveness of cooling needs to be explored. Radiation damage (especially from neutral particles) may represent a significant issue and needs to be considered. Such an assessment is

also important for other detectors, such as the mRICH, which are located closer to the beam line and which can be potentially readout by SiPMs. LAPPDs could turn out to be the ultimate solution, but as they are currently under development and their performance and reasonable scale availability all need to be proven, we could not consider them a potential baseline candidate, yet (although more expensive commercial MCP-PMTs could be used).

DAQ: The large number of photon-sensor channels that needs to be readout imposes requirement for a compact, modular, and fast data-acquisition system (DAQ).

As mentioned above, the dRICH performance (estimated by detailed simulations and event-based reconstruction) as well as the critical features of the key components of the detector need to be assessed and validated by real measurements. For this reason, the design of the small-scale prototype, we proposed in 2017, was further fine-tuned. The main considerations taken into account are that the prototype must:

- mimic the performance of the dRICH components, and/or permit to evaluate them in a direct way (minimizing modeling and assumptions).
- be cost effective (trade-off of small scale, flexibility, and measurable quantities).

The prototype vessel is a 1-m long cylinder of a radius of 0.3 m. This geometry is the result of the following two considerations:

- a reasonable number of photoelectrons per particle in the gas ring (order of 10); this number depends almost linearly on the thickness of the gas and, therefore, on the length of the vessel.
- the probability to catch the aerogel ring (20-cm radius), which is needed to estimate its angular resolution; this parameter constraints the transverse size of the vessel.

The minimum surface area of the photon detector must be around 8x8 cm^2 to guarantee an almost 100% coverage of the gas ring (radius of approx. 4 cm). A photo-sensor pixel size of 3 mm will keep the angular-digitization (or pixel) uncertainty comparable to or smaller than other uncertainties (important for the study of intrinsic sources of uncertainties in the aerogel) and will reduce the chance to detect multiple photoelectrons in a single pixel for the gas ring (which is important for an accurate estimate of the number of Cherenkov photons)

Other components of the prototype are a small spherical mirror with a radius of about 2 m, a support (isolated from the gas) for the aerogel tiles, and a tiny slab of filter (*e.g.,* Lucite). The prototype configuration was modeled in GEMC/Geant4. An example of a simulated event is shown in Fig. 2.2.2 and Fig. 2.2.3.

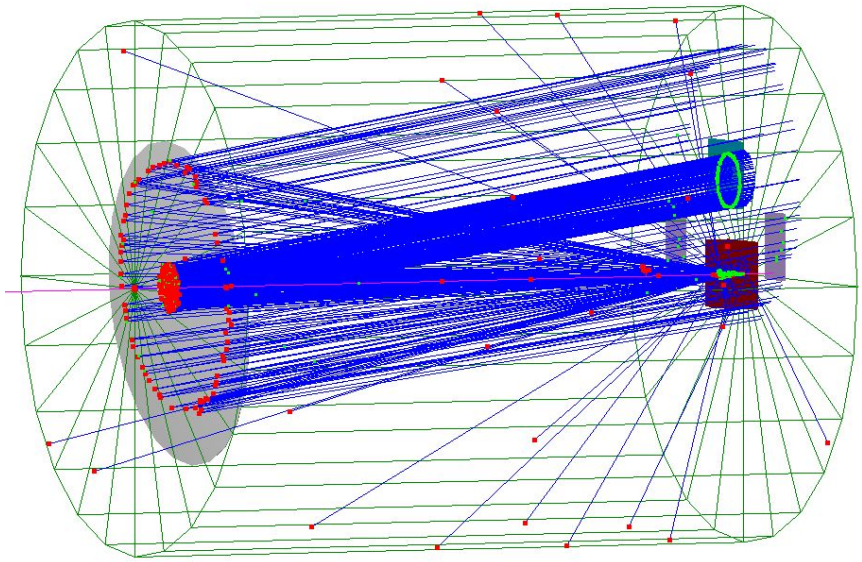

Figure 2.2.2: Simulation of a single event (with momentum above the aerogel and gas thresholds) in the dRICH prototype (length of 1 m, radius of 0.3 m). The particle travels from right to left. The reflective mirror is on the left-hand side and is shown in grey. The photo-sensors are located on the right-hand side and are also shown in grey. Cherenkov photons produced in the aerogel (dark red) and the gas (all along the cylinder) are reflected by the spherical mirror toward the photon detectors.

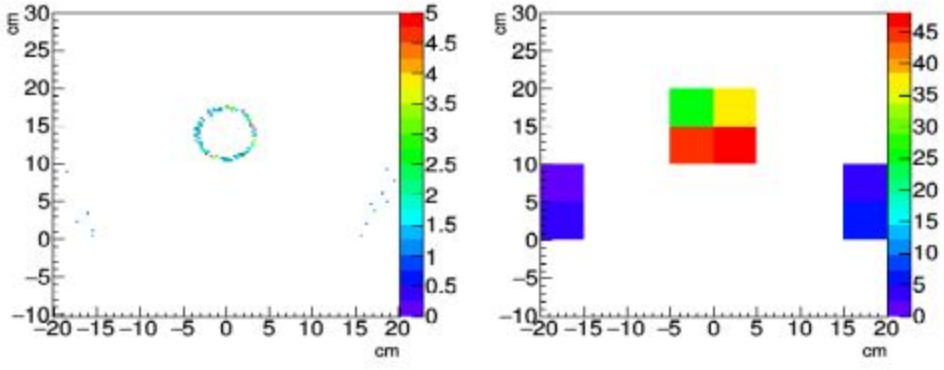

Figure 2.2.3: Simulated hits of Cherenkov photons on the photodetectors for the event shown in Fig. 2.2.2: the small gas ring is be fully reconstructed by 4 5x5 cm^2 SiPMs, while only two opposite small arcs of the aerogel rings can be covered by photosensors of the same area (configuration shown in Fig. 2.2.2).

The main sources of uncertainty contributing to the single-photoelectron (1 p.e.) angular resolution were estimated in the GEMC/Geant4 simulation and are reported in Table 2.2.2. It is evident that the aerogel chromatic error (and possibly forward and Rayleigh scatterings) is an

important parameter that needs be accurately investigated. According to the simulation, the expected number of p.e. per ring in the gas is about 14, which corresponds to 3 – 4 p.e. on a 5x5 cm^2 SiPM, while for the much larger aerogel the expected p.e. on a single SiPM is about 0.8. In the gas, the resolution can thus be evaluated for each single event, but for the aerogel ring a sample of cumulative events is required.

1 p.e. Uncertainty [mrad]	Aerogel	C_2F_6 gas
Chromatic	3.7	0.9
Emission	0.2	0.9
Pixel	0.9	1.0

Table 2.2.2: Estimates of the main uncertainties contributing to the single photo-electron angular resolution. The values are obtained by means of GEMC/Geant4 simulation of the dRICH prototype.

2.2.2 Future

2.2.2.1 What is planned for the next funding cycle and beyond? How, if at all, is this planning different from the original plan?

The second half of 2018 was a transition period for the dRICH activities. In May 2018, Alessio Del Dotto completed his EIC postdoctoral fellowship with a comprehensive analytical and Monte-Carlo design of the dRICH. His new position will, however, make it possible to remain involved in advisory role in the software aspect of the project. At the beginning of 2019, the new EIC postdoc Luca Barion will start working on the mRICH and dRICH projects with an emphasis on hardware development.

The plan for 2019 is to continue with the development of the dRICH small-scale prototype. This activity will be carried out in strong synergy with the development of the readout electronics (*e.g.*, from Hawaii University) and sensors for the mRICH prototype. In fact, everything accomplished on sensor and electronics for the mRICH, applies to the dRICH prototype.

Specifically, our planned activities include:

1. Design finalization and implementation of a small-scale, flexible prototype that can host: aerogel, gas, mirror and either a matrix of SiPMs or other photon detectors (such as GEM based sensors, which are suitable for the gas-only RICH option).
2. Support of the development of a DAQ for the SiREAD chip. This will be done in synergy with the mRICH colleagues and in collaboration with JLab. Our responsibility is the integration and related tests of the back-end readout electronics.
3. Design finalization, construction, and tests of a SiPM matrix with proper cooling and thermal stability. Evaluation single-photon performance of existing SiPMs at the radiation levels expected at the EIC and study mitigation solutions for SiPM, in particular regarding temperature control [Cal18] in conjunction with micro-cell geometry and fast signal component pickup. Assessment of ongoing SiPM developments towards

radiation-hard solutions.

4. Setup of a pulsed-laser test bench for characterization of optical sensors in conjunction with activity 2 above. A test bench will be useful for the evaluation and validation of readout electronics, for the definition of the best working parameters in preparation for beam tests, and for the evaluation of sensors radiation tolerance during future irradiation campaigns.

An article describing the developed event-based Cherenkov-angle reconstruction will be circulated in the first half of 2019.

2.2.2.2 What are the critical issues?

The procurement of samples of aerogel with an index of refraction of 1.02, may represent a critical issue due to the potential lack of providers. It is worth to point out that the dRICH performance strongly depends on the quality and stability of the aerogel radiator. So far, only the HERMES and the LHCb experiments have adopted dual-radiation (aerogel and gas) RICH detectors: the HERMES RICH (that used the Matsushita hydrophobic aerogel) was successful, but it did not require maximum performance from the aerogel. The LHCb RICH (that used Dubna hygroscopic aerogel) had significant performance issues. The procurement and the comprehensive study of the performance of different aerogels are, therefore, essential for the dRICH success.

The limited amount of funding may also influence the design of the prototype.

References:

[Dot17] A. Del Dotto et al., “Design and R&D of RICH detectors for EIC experiments”, NIM A 876 (2017) 237-240

[Ili18] Y. Ilieva et al., “Particle Identification for a future EIC detector”, J. Instr., 13 (2018)

[Hor17] T. Horn et al., “The Aerogel Cherenkov Detector for the SHMS magnetic spectrometer in Hall C at Jefferson Lab”, Nucl. Instrum. Meth.A 842 (2017) 28-47 (arXiv:1607.05264)

[Chr99] L.G. Christophorou and J.K. Olthoff, “Electron Interactions With Plasma Processing Gases: An Update for CF4, CHF3, C2F6, and C3F8”, Journal of Physical and Chemical Reference Data 28, 967 (1999)

[Cal18] M. Calvi et al., “Single photon detection with SiPMs irradiated up to 10^{14} cm^{-2} 1-MeV equivalent neutron fluence’

2.3 Modular Aerogel RICH (mRICH)

This lens-based, compact, and modular Aerogel RICH detector provides hadron PID capability from 3 to 10 GeV/*c* (for π/K separation) and electron PID (for e/π separation) below 2 GeV/*c*. The details of this detector design can be found in the eRD14 FY19 proposal and in our mRICH publication [1]. In this report, we highlight progresses made on the mRICH project since July of

2018 and describe further activities planned for FY19.

2.3.1 Past

2.3.1.1 What was planned for this period?

The planned major activities for this period included (1) data analysis of the second mRICH prototype beam test at Fermilab in Summer of 2018; (2) implementation of an mRICH detector in the Forward sPHENIX and in the BeAST EIC detector designs; (3) the study of the mRICH performance in the JLab EIC detector design using Pythia events.

2.3.1.2 What was achieved?

The achievements for the mRICH project during this report period include: (1) a near completion of the data-quality assurance (QA) analysis of the second mRICH beam test at Fermilab from June 25 to July 6, 2018 (see Fig. 2.3.1 for examples of ring images from this analysis); (2) mRICH detector array implementation in the Forward sPHENIX detector (see Fig. 2.3.4) using the Fun4All framework (this work has been included in a LOI document which was submitted to LRD from the sPHENIX Collaboration); (3) mRICH performance study in JLEIC using simulated events from Pythia event generator, as shown on Fig. 2.3.5.

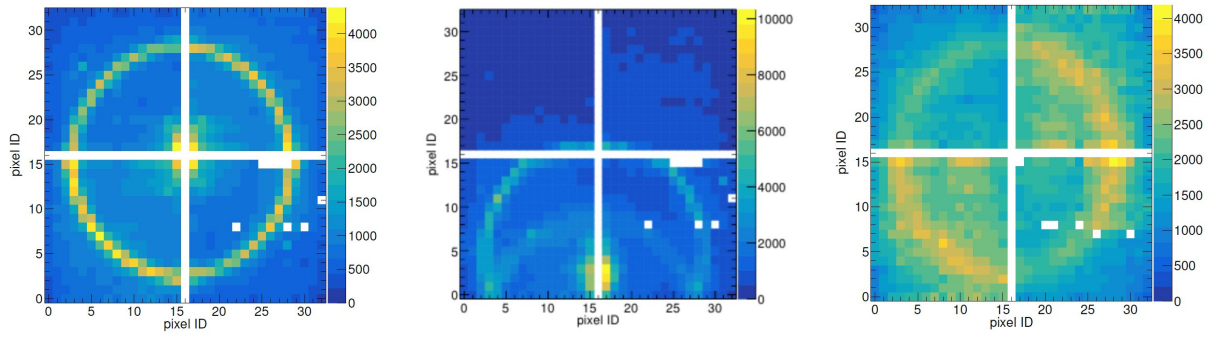

Figure 2.3.1: Examples of cumulative ring images from the second mRICH prototype beam test. **Left**: ring images formed by the 120-GeV primary proton beam incident on the center of mRICH. **Middle:** ring images from the 120-GeV primary proton beam incident at an angle of 11° toward the lower section of mRICH. **Right:** images from an 8-GeV meson run. Hamamatsu H13700 PMTs were used in these test runs. Note the lower noise level in the cooled SiPMs.

For the first time, we used SiPM matrices (from Hamamatsu, 16 x 16 matrix, 3cm x 3cm pixel size) to read out signals from mRICH. The successful implementation and operation of the SiPMs was indeed a significant achievement in this R&D study. SiPMs were used due to the requirement of photosensors functioning in a high magnetic field in the EIC experiments. Figure

2.3.2 shows the assembling of SiPM matrices mounted on cooling blocks (left picture) and the cooling system used for this test (right picture). The test data were taken with the 120-GeV primary proton beam at cooling temperature of -30^0 C, -20^0 C, -10^0 C, 0^0 C and room temperature. Figure 2.3.3 shows three examples of cumulative ring images from this test. Detailed data analysis is ongoing and is one of the major activities proposed for FY19 period.

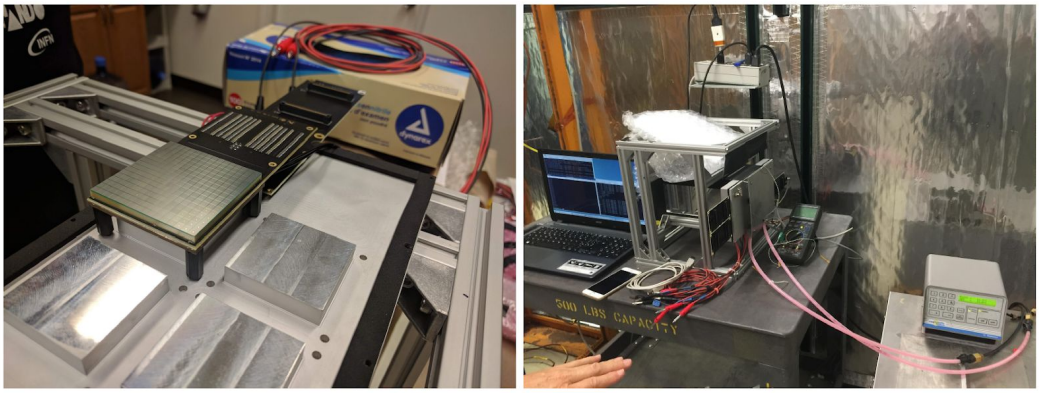

Figure 2.3.2: SiPM matrices setup (left picture) and the cooling system, liquid cooling (right picture). Only three matrices were available for this test.

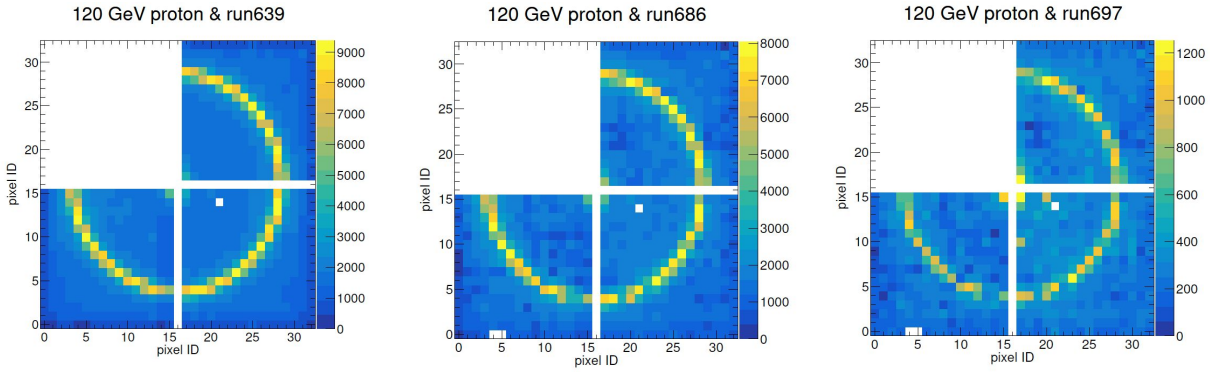

Figure 2.3.3: Examples of cumulative ring images from the second mRICH prototype beam test using three SiPM matrices. **Left:** at a cooling temperature of -20^0 C. **Middle:** at a cooling temperature of 0^0 C. **Right:** at room temperature.

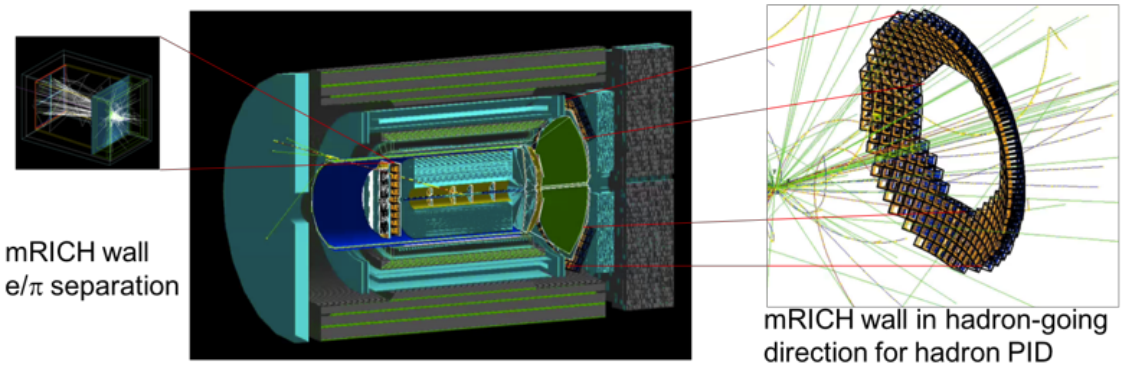

Figure 2.3.4: The mRICH subsystem implemented in the Forward sPHENIX detector design. The individual mRICH modules can be mounted projectively toward the interaction point.

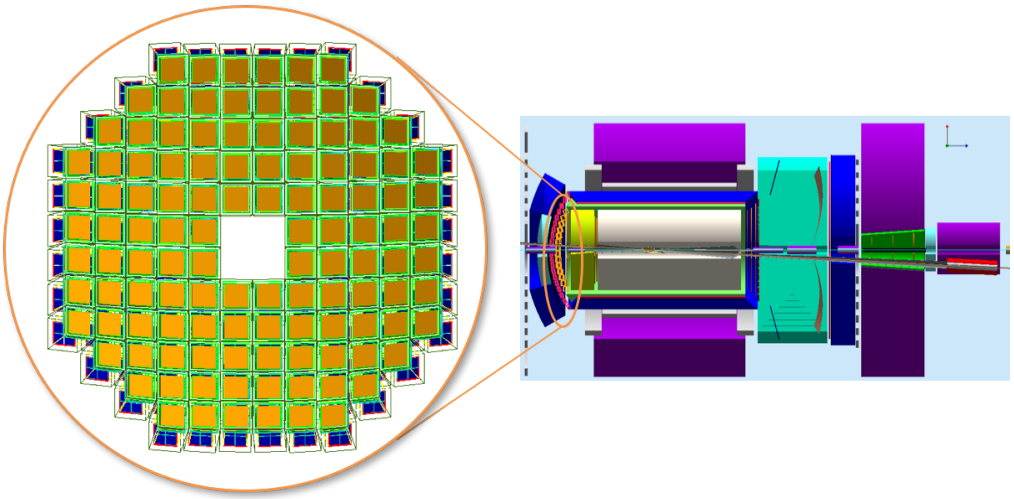

Figure 2.3.5: The mRICH subsystem implemented in GEMC within the JLab detector design (shown on the right). The individual mRICH modules can be mounted projectively toward the interaction point.

2.3.1.3 What was not achieved, why not, and what will be done to correct?

We were not able to take mRICH data with beam hodoscopes during the second beam test because of a readout issue. We are currently assessing the impact of the lack of hodoscope signals on the meson beam data set. The main concern is whether we are able to determine the beam incident direction.

2.3.2 Future

2.3.2.1 What is planned for the next funding cycle and beyond? How, if at all, is this planning different from the original plan?

The major activity in the next funding cycle is to successfully complete the second mRICH beam test data analysis and to publish the results. The mRICH group plans to work with the DIRC

team to study optical degradation of acrylic-based Fresnel lens in Spring 2019. An initial test done by Greg Kalicy at BNL using ^{60}Co indicated that the reduction of optical transmission of acrylic Fresnel lens is not significant for mRICH application (see Section 2.4.1.2 for details). A confirmation measurement is necessary in order to address the concern of radiation hardness of acrylic-based Fresnel lens by the EIC R&D Committee once for all. In the coming budget period, the mRICH group also plans to work with the dRICH team to have a joint beam test at Fermilab.

2.3.2.2 What are the critical issues?

One critical issue for the continued mRICH prototype study is to solve the readout problem of the mRICH beam hodoscope and the readout integration to the photosensor readout. Another critical issue is to acquire more samples of aerogel blocks given the limited funding support. More samples will allow us to make systematic study of the mRICH performance and the associated uncertainties of PID performance.

References

[1] C.P. Wong, et. al., *Modular focusing ring imaging Cherenkov detector for electron-ion collider experiment,* NIM A 871, 13 (2017).

2.4 High-Performance DIRC

A radially-compact detector based on the DIRC (Detection of Internally Reflected Cherenkov light) principle is a very attractive solution for the EIC, providing particle identification (e/π, π/K, K/p) over a wide range of angles and momenta. The DIRC is a type of RICH detector using rectangular-shaped radiators made of synthetic fused silica that also function as light guides, transporting the Cherenkov photons to an expansion volume, where they are recorded by an array of photon sensors. During the photon transport the emission angle of Cherenkov photons with respect to the particle track is maintained and can be reconstructed from measured parameters. DIRC detectors are inherently 3D devices, measuring the image location on the detector surface (*x, y*) and the time of arrival of each photon (*t*).

The High-Performance DIRC design developed for the EIC detector is inspired by the original DIRC detector used by BaBar and by the PANDA Barrel DIRC detector currently in development. The baseline design, implemented in a Geant4 simulation, is shown in Fig. 2.4.1a. The radiators are 4.2-m long each, with a cross-section of 17 mm x 32 mm. Eleven such bars are placed side-by-side, separated by a small air gap, into a light-tight bar box. The 16 bar boxes are arranged in a barrel with a radius of 1 m around the beam line. Mirrors are attached to one end of each bar. On the opposite end, where photons exit the bar, a special 3-layer spherical lens is coupled to a large prism-shaped expansion volume, made of synthetic fused silica. A closeup view of this region is shown in Fig. 2.4.1b. The prism has a 38° opening angle, and dimensions 285 mm x 390 mm x 300 mm. The detector plane of each prism is covered by 3 mm x 3 mm pixels for a total of about 208k channels to record the location and arrival time of the Cherenkov photons.

A key component to reach the required performance is a special 3-layer spherical compound

lens. A schematic and photos of a prototype lens, procured in 2015, are shown in Fig. 2.4.1c. This lens contains a layer of the high-refractive index material Lanthanum crown glass (NLaK33), sandwiched between two layers of synthetic fused silica. The two radii of the 3-layer lens were optimized to remove aberrations present in standard lenses by first defocusing and then focusing the photons to create a flat focal plane, matching the geometry of the prism expansion volume.

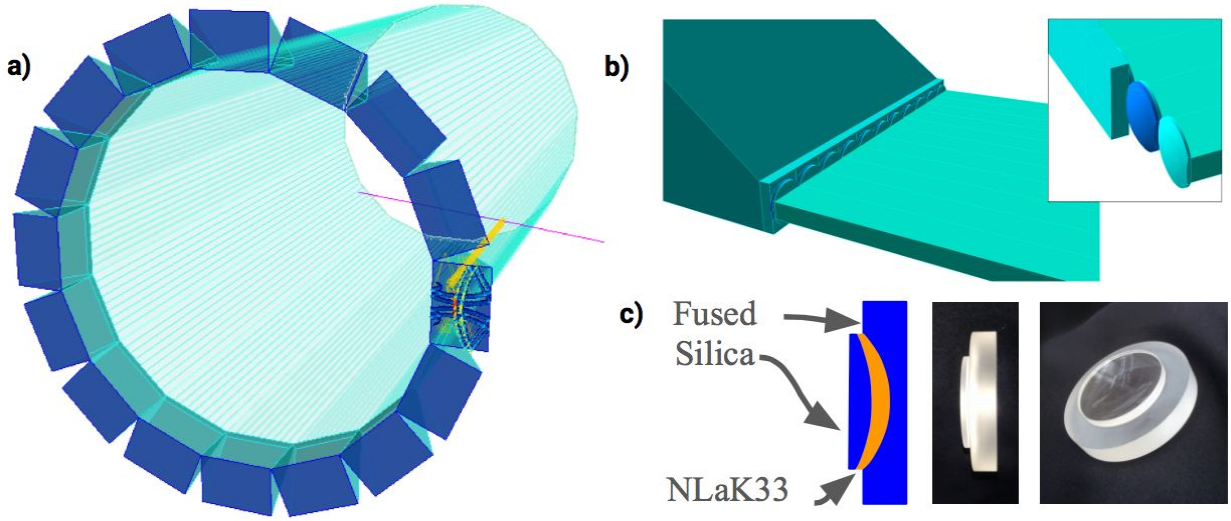

Figure 2.4.1: a) Geant4 geometry for the simulation of the high-performance DIRC. b) Detail showing the fused silica prism expansion volume, a row of spherical three-layer lenses with high index of refraction and the radiator bars. The insert shows the individual lenses and layers of the spherical lens system. c) Schematic and photos of the 3-layer lens prototype.

2.4.1 Past

2.4.1.1 What was planned?

The key hardware-related activity planned for the second half of FY18 and the beginning of FY19 was to perform a detailed radiation hardness study of the various optical DIRC materials by irradiating samples in a ^{60}Co source at BNL. Two prototype lenses, made with alternative high refractive index materials, were suppose to be designed and ordered. Several simulation studies were planned. Synergetic work with the PANDA Barrel DIRC focused on evaluating design options with the DIRC prototype in a CERN test beam in July/August 2018.

2.4.1.2 What was achieved?

A successful radiation hardness study was performed at BNL, and five materials were tested up to 750 krad.

Discussion are underway to finalize the purchase of two custom-made 3-layer lenses using sapphire and PbF_2 as the middle layer, respectively.

The successful beam test of the PANDA Barrel DIRC prototype identified the potential for a significant reduction in the number of sensors required to cover the detector plane.

Radiation Hardness Measurement

The determination of the radiation hardness of materials is an important aspect of the EIC DIRC R&D. Synthetic fused silica, which is used for most of the optical components in all DIRC systems, was already extensively tested for the BaBar and PANDA DIRC counters and proved to be radiation hard. However, the middle layer of the 3-layer lens was made, in all prototypes up to now, of a high-refractive index lanthanum crown glass, NLaK33, and our first radiation tests strongly suggested that this material may not be suitable for the final design. Several materials were studied as potential alternatives to NLaK33, and so far sapphire and PbF_2 are the leading candidates. All potential candidates have to be tested for radiation hardness.

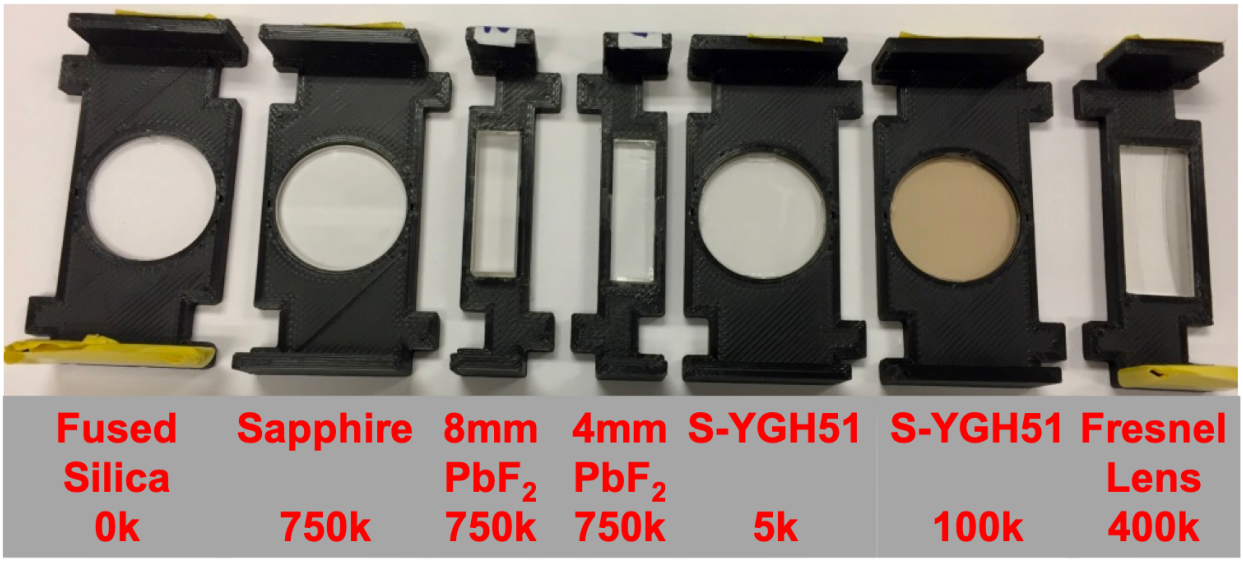

Figure 2.4.2: Samples of materials after irradiation in a ^{60}Co source with corresponding deposited doses.

A commonly used source for studies of radiation hardness of optical materials is ^{60}Co. Following the July 2017 and the January 2018 recommendations by the R&D review committee, we prepared a dedicated setup for radiation hardness measurements with the ^{60}Co source at the BNL radiation facility. Samples of PbF_2, sapphire, S-YGH51 (Lanthanum crown glass, alternative to NLaK33)), as well as acrylic glass, used for the current mRICH Fresnel lens prototype, were exposed to accumulated doses of up to 750 krad. Fig 2.4.2 shows a photo of samples tested at BNL after the completion of the irradiation program, as well as a Fused Silica sample, never irradiated and used as a reference in the transmission measurements. A visible colour change was observed only for the S-YGH51 sample.

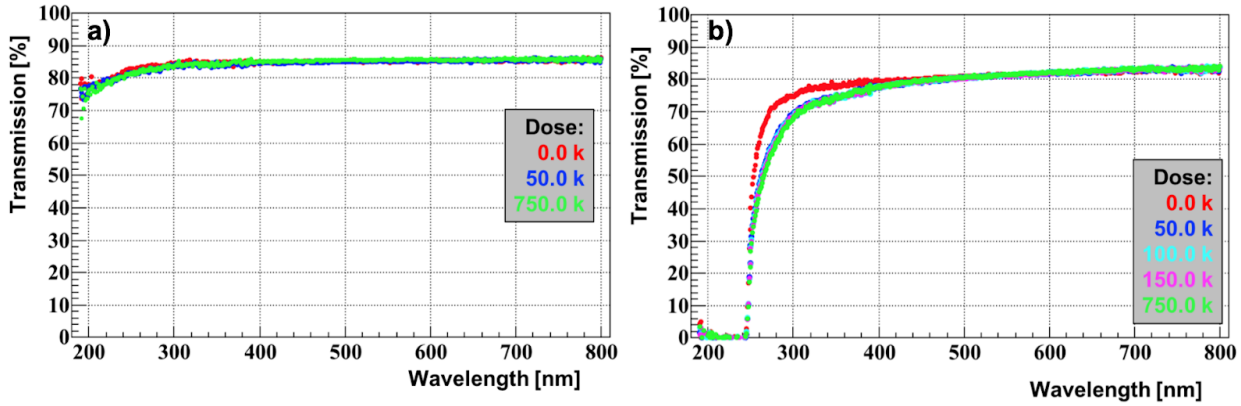

Figure 2.4.3: Measured transmission (not corrected for Fresnel losses) through the 2 mm-thick sapphire (a) and 8mm-thick PbF_2 (b) sample as a function of wavelength for selected amounts of deposited gamma ray dose from ^{60}Co.

The radiation damage is quantified by measuring the transmission in the 190-800 nm range in a monochromator. Two light sources with different measurement precision are used in the process, resulting in a precision of ±0.5% for the 390-800 nm range and ±1.2% below 390 nm. The results of the radiation hardness test for a 2 mm-thick sapphire sample are shown in Fig. 2.4.3a. Only three transmission measurements are shown: before irradiation, after the first 50 krad irradiation step, and after irradiation with the full dose. There is no significant transmission loss even after the dose of 750 krad. Figure 2.4.3b shows results for the 8 mm-thick PbF_2 sample. We observe a small transmission loss below 400 nm. The saturation of the absorption band happened, however, already below the first 50 krad step and we observed no further changes, even after reaching 750 krad.

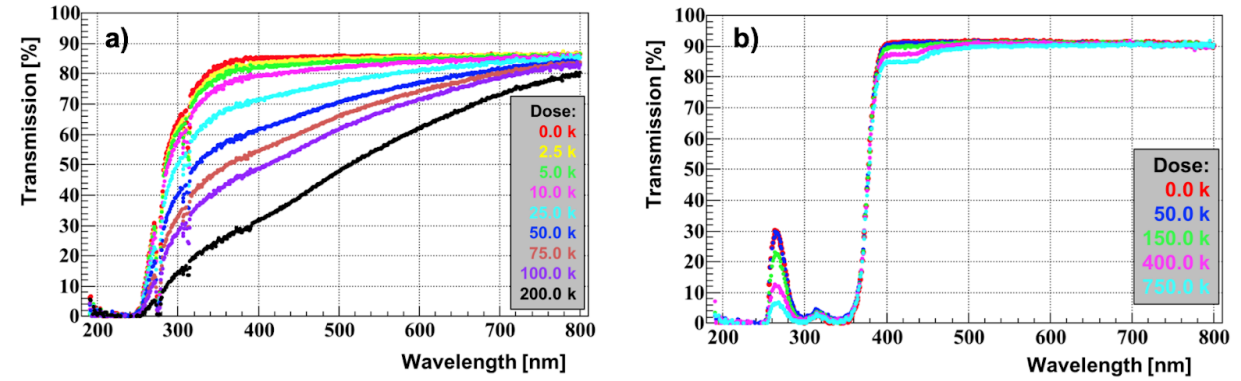

Figure 2.4.4: Measured transmission (not corrected for Fresnel losses) through the 2 mm-thick S-YGH51 glass (a) and 2 mm-thick Fresnel lens (b) sample as a function of wavelength for selected amounts of deposited gamma ray dose from ^{60}Co.

The results for the 2 mm-thick S-YGH51 Lanthanum crown glass sample are shown in Fig. 2.4.4a. Smaller irradiation doses for each step were selected based on earlier calibration

measurements. We observe a significant deterioration of transmission for the full wavelength range. After 200 krad deposited dose we observe a transmission drop from 85% to 32% at 400 nm. The loss rate appears to be approximately linear, 0.5% per krad at 300-400 nm and 0.25% per krad at 500 nm. As reported earlier, the S-YGH51 glass is recovering part of the transmission loss with time. A detailed quantification of the recovery process is in progress. Figure 2.4.4b shows results for the 2 mm-thick acrylic mRICH lens sample. A small drop of transmission was observed below 500 nm but in general this material proved to be surprisingly radiation hard even after a dose of 750 krad.

Based on past experience, we anticipate that a follow-up radiation hardness measurement, with an extended dose range and a possible evaluation of radio-luminescence, will be needed in FY19.

2018 test beam at CERN

Although this activity was not funded during the current period, the results of our collaboration with the PANDA Barrel DIRC group, and the outcome of their 2018 beam test at CERN, should be noted.

Experimental validation of the new design ideas are important for the DIRC in the EIC R&D program. Since not all of the required components of the high-performance DIRC baseline design are available yet (such as sensors with small pixels, fast readout electronics, full-length radiators, *etc*) the collaboration with the PANDA Barrel DIRC group is used to evaluate the performance of the specific design options for the High-Performance DIRC.

The test beam at CERN in July/August 2018 was primarily focused on the validation of the PID performance of a cost-saving PANDA Barrel DIRC design option with reduced MCP-PMT coverage. The prototype featured a single narrow synthetic fused silica radiator bar, coupled to the 3-layer spherical lens, which was coupled to the synthetic fused silica prism expansion volume with a 33° opening angle, identical to the 2017 setup. However, while the 2017 prototype featured a 3x4 array of MCP-PMTs covering the entire backplane of the prism expansion volume, the 2018 prototype, shown in Fig. 2.4.5a, used a 2x4 MCP-PMT array, covering only ⅔ of the prism backplane. An example occupancy plot for the new sensor arrangement is shown in Fig. 2.4.5b. The data analysis is still ongoing but first results are very encouraging. Figure 2.4.5c shows the π/p separation power as a function of the beam polar angle. The observed PID performance of the 2x4 MCP-PMT array meets the PANDA requirements. Although the observed lower photon yield, caused by the limited sensor coverage, is expected to lead to a loss of π/p separation power, the measured performance in 2018 was consistently similar to or better than in 2017. A possible explanation is that a loss of photons in the region of overlapping hit patterns, near the sides of the prism, has a reduced effect on the PID performance for the time-based imaging reconstruction. The direct comparison to 2017 is, however, complicated by the fact that several parameters were changed. The laser pulser calibration method was improved for 2018 and the performance of the TRB/PADIWA-based readout electronics was about 10% better in 2018. Further analysis is needed to separate the effects of the photon yield and the timing precision.

However, due to the substantial cost savings, the 2x4 MCP-PMT array design has been selected for the PANDA Barrel DIRC construction and should be considered for the High-Performance EIC DIRC as well.

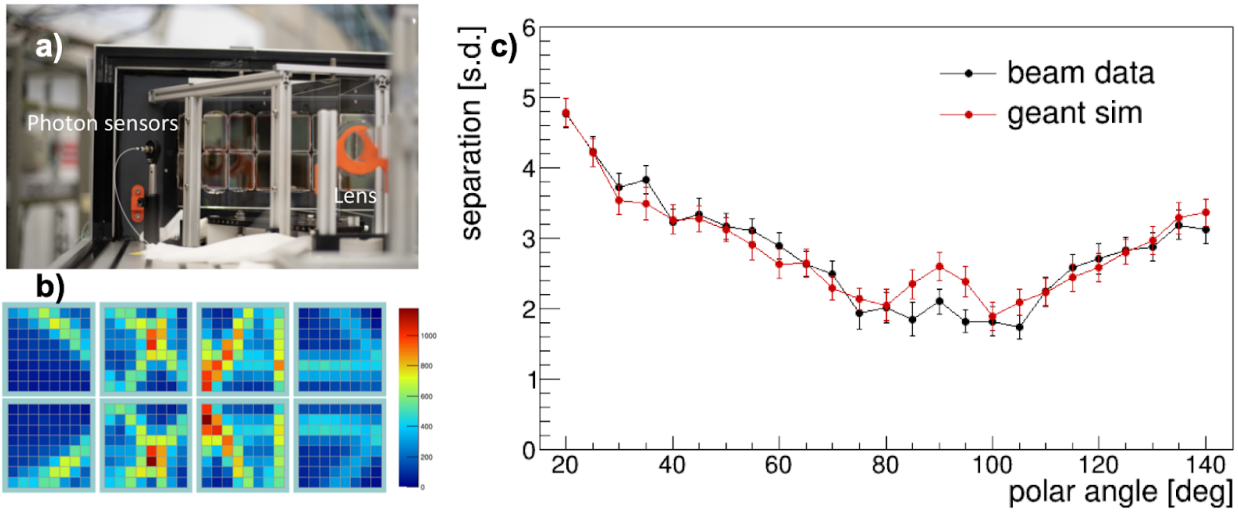

Figure 2.4.3: a) Photo of the MCP-PMT arrangement in the PANDA Barrel DIRC 2018 prototype at CERN. b) Distribution of the number of detected hits per MCP-PMT pixel from 50k pions at a polar angle of 20° and a momentum of 7 GeV/*c*; c) π/p separation power as a function of the beam polar angle.

2.4.1.3 What was not achieved?

The process of purchasing two prototype lenses is in progress and is expected to be finalized in Spring 2019.

Due to limited available FTEs the scope of the simulation studies had to be reduced and focussed on validating the usability of sapphire and PbF_2 in the 3-layer lens, prior to completing the design of the prototype lenses. The implementation of the High-Performance DIRC baseline design into JLab-EIC, EIC-sPHENIX, and the BeAST detector simulation frameworks is being prepared to be performed in the most FTE-efficient manner, by making use of synergies with other EIC R&D detector and software groups. Although the planned effort on the time-based imaging for the EIC DIRC had to be postponed due to the FTE issues, some progress was made due to synergies with the GlueX DIRC group.

2.4.2 Future

2.4.2.1 What is planned for the rest of FY19? How, if at all, is this planning different from the original plan?

Candidate materials for the High-Performance DIRC and the mRICH lens will be studied further in terms of radiation hardness. That includes additional studies of materials already tested as

well as several new materials with a goal to publish results around the end of FY18.

Two new prototype lenses with sapphire and PbF_2 will be build and will have to be studied in case of optical properties on the test bench. Laser setup build for the 3D mapping of the focal plane will be upgraded to improve measurement precision.

The activities on the detailed GEANT simulation and the time-based imaging are being slowed down because of not enough manpower. Current and future work will be shared between CUA and GSI group however until hiring of a new PostDoc hardware activities will have priority.

Preparations for the planned transport of the PANDA Barrel DIRC prototype to the US in the next fiscal year are in progress and will continue.

2.4.2.2 What are the critical issues?

The radiation-hard 3-layer lens is a core element of the High-Performance DIRC design. The significant radiation damage of the NLaK33 material at a modest gamma dose and the subsequent transmission recovery need to be studied in detail. Alternate, radiation hard, materials were identified but they present challenges for the manufacturing process. That is why it is crucial to build prototypes with two main candidates, PbF_2 and sapphire. To facilitate the evaluation of the DIRC performance in combination with other PID systems, the optimization of the DIRC design and the implementation in existing detector simulation frameworks, are very important.

2.5 High Resolution Time-of-Flight

There were no funded activities during this period.

3. Photosensors and Electronics

3.1 Summary

The main objective of this R&D effort during the period July – December 2018 was to continue to identify and assess suitable photosensor solutions for the EIC Cherenkov Detectors and to develop electronics solutions for the readout of the Cherenkov detectors prototypes for beam tests. Ultimately, in the long term, this R&D work will allow us to make a recommendation about the best photosensors and electronics solutions for the PID detectors in EIC implementation.

3.2 Sensors in High-B Fields

3.2.1 Past

3.2.1.1 What was planned for this period?

In this reporting period we planned to (a) construct and commission a fast laser system for timing measurements, (b) upgrade the High-B setup with timing electronics, (c) commission the system, (d) study ion backflow as a function of high voltage and magnetic field, as recommended by the review committee in their January 2018 report, and (e) study the gain and efficiency dependence of a 10-μm pore-size Planacon on the voltage between the photocathode and the first micro-channel plate (MCP).

3.2.1.2 What was achieved?

In Spring and Summer 2018 an optical box housing the 404-nm PiLas laser was designed and constructed. The box is equipped with an interlock switch to comply with JLab safety rules. The laser light is routed to the front window of the MCP-PMT entirely via optical fibers so that there is no open-space distribution of light. Figure 3.2.1 shows a schematic diagram of the laser system.

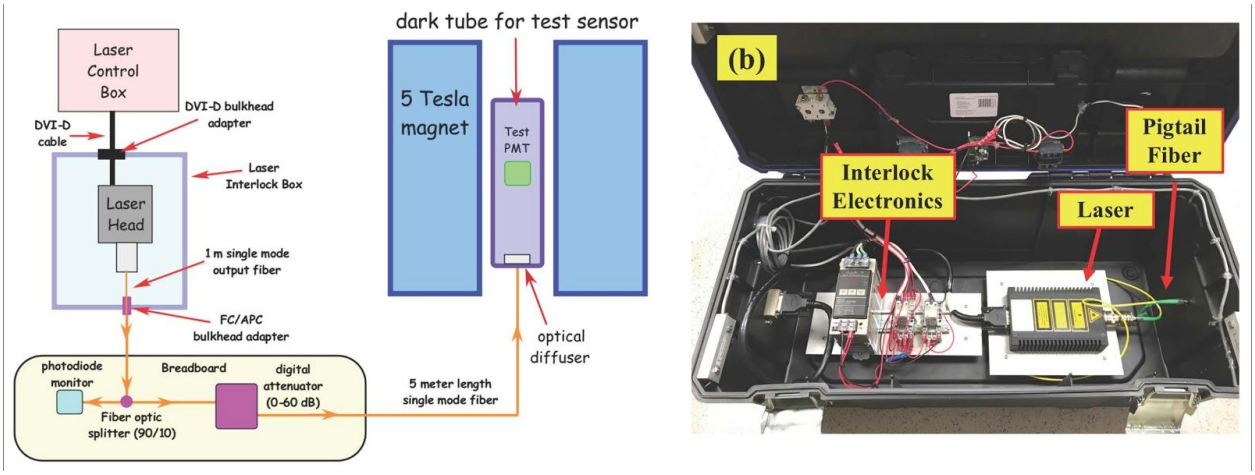

Figure 3.2.1: Left: Schematic diagram of the laser-light distribution. The laser head is mounted in a Laser Interlock Box and is controlled through a Control Box[1]. The laser light is split by means of a fiber-optic splitter as follows: 10% is directed to a digital attenuator and then to the dark box housing the MCP-PMT, whereas 90% is directed to a monitoring photodiode[2]. The splitter, the photodiode, and the digital attenuator are all located outside of the Interlock Box for easy access and attenuation changes. In the dark box, the attenuated laser light is diffused, as was done with the light generated by a pulser driven LED in our previous measurements. **Right:** A photograph of the Interlock Box. One can see the interlock electronics, the laser head, and the fiber output of the laser head.

The laser system was assembled and tested in the JLab Detector lab under the supervision of C. Zorn. The system was moved to the High-B facility and commissioned there in July 2018. For

[1] Controller EIG2000DX, Advanced Laser Diode Systems.
[2] ThorLabs High-Speed Fiber-Coupled DET025AFC.

the commissioning, the laser was operated at tune of 50% and frequency of 1 kHz. The external attenuation provided by the digital attenuator and needed to operate the system in a single photo-electron mode was found to be 15 dB. To test the laser system settings, and especially the attenuation, we compared the MCP-PMT spectrum to the one obtained with LED light. Figure 3.2.2 shows the comparison. The fit parameters μ and Q_1, which quantify the ratio of single-photoelectron and pedestal events ($\mu = N_{1phe}/N_{ped}$) and the PMT gain, respectively, are consistent between the LED and the laser lights. The value of μ is also consistent with the ratio N_{1phe}/N_{ped} obtained by counting triggers and signals one-by-one using an oscilloscope.

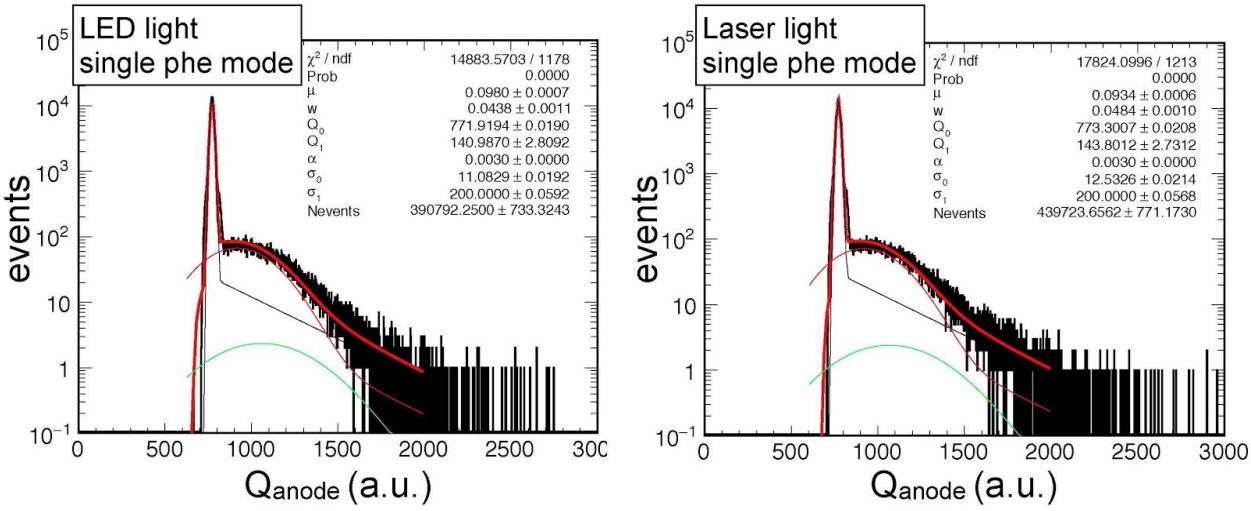

Figure 3.2.2: Comparison between the response of the Planacon MCP PMT to LED light (**left**) and Laser light (**right**) in single-photoelectron settings. The comparison demonstrates that the laser setup has been commissioned successfully.

For timing measurements, a CAEN TDC V775 (on temporary loan from Hall A at JLab) was installed and implemented in the Data Acquisition. We have started to work on the commissioning of the TDC for timing measurements – this activity will be completed in Spring of 2019. A higher resolution TDC (CAEN V1290) will be procured in early 2019 for the Summer-2019 measurements.

Our Summer 2017 results showed different variations of the relative gain (fit parameter Q_1) and relative N_{1phe}/N_{ped} (fit parameter μ) with B-field at fixed angle *θ*. While at large *θ* $Q_1(B)/Q_1(0)$ increased, μ(B)/μ(0) decreased. Since Q_1 quantifies the number of electrons in a detected avalanche, whereas μ quantifies the number of detected avalanches, we refer to μ as *efficiency*. A possible explanation of the Summer-2017 observed efficiency trend at large *θ*, would be that there is a loss of some photoelectrons in the gap between the photocathode and the first PMT since larger *θ* angles correspond to larger B_{perp} and, thus, to a smaller radius of curvature of trajectory of the photoelectron. In Summer 2018, we scanned the evolution of the relative efficiency with *B* over a more comprehensive number of *θ* angles, *i.e.*, 0°, -5°, -10°, and -20°, and two values of HV: -2.7 kV and -2.6 kV. As the extracted value of μ is very sensitive to the quality and the properties of the fit to the event distribution over Q_{anode}, we developed several

alternative methods to quantify the MCP-PMT efficiency. We typically take data at constant light intensity in a single-photoelectron (spe) mode, thus the total number of signals is by far dominated by spe signals and one can alternatively quantify the PMT efficiency, ε, as a ratio of the total number of signals to the number of pedestals, N_{sig}/N_{ped}. In Fig. 3.2.3, we show the relative efficiency ε(B)/ε(0) for different sensor orientations, *θ,* with respect to the B-field axis. The relative gain, G(B)/G(0) is also shown.

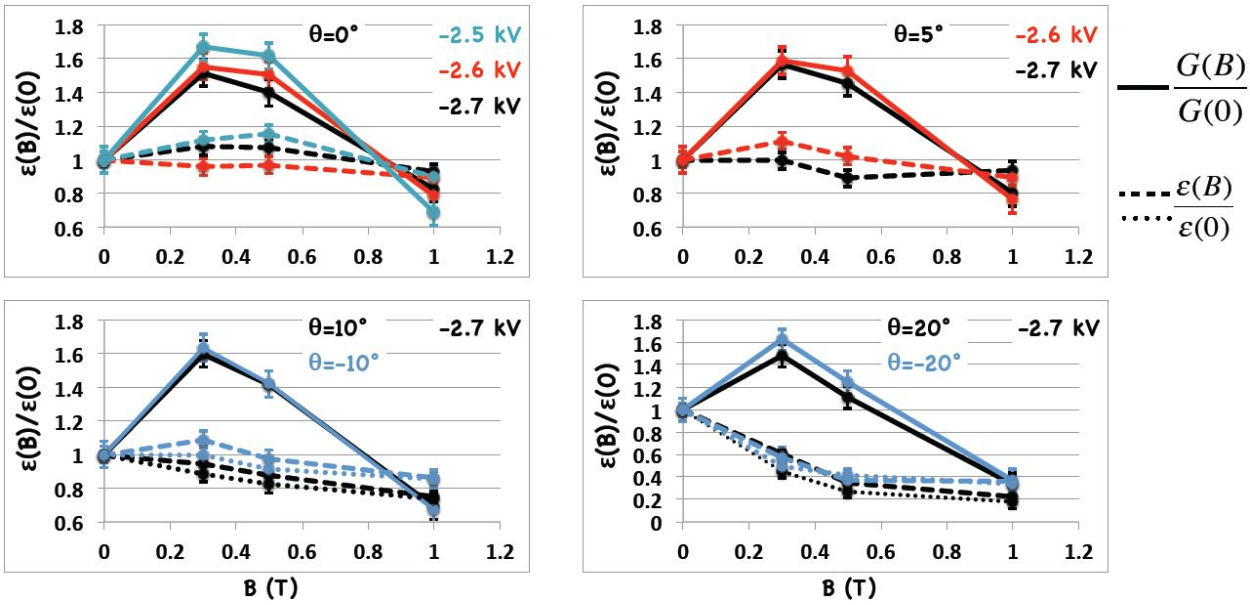

Figure 3.2.3: Relative gain (solid lines) and relative efficiency (dashed and dotted lines) as a function of B-field magnitude for various sensor orientations and high voltages. The dashed and dotted lines at 10°, and 20° are obtained from two alternative methods and visualize the uncertainty of the extraction of the relative efficiency.

Overall, one sees that the relative efficiency is less sensitive to the B-field magnitude than the relative gain at small angles. While at 0° and 5° the efficiency is practically constant up to 1 T, it slowly decreases to 80% at 1 T at 10°. The largest effect is observed at the largest angle we can access in the setup, ±20°, where the efficiency continuously drops to 30% at 1 T. At this angle, the data show unambiguously that the efficiency decreases even if the gain increases at 0.3 T and 0.5 T. This observation is consistent with our results from Summer 2017. It would be interesting to map in more detail the angular range between 10° and 20° to identify at which angle the transition from slow to fast decrease occurs. Such measurements would be pursued in Summer 2019.

To study the effect of the potential difference between the photocathode and the first MCP on the PMT efficiency and identify the extent to which the drop in efficiency at ±20° could be recovered by increasing this potential difference, we commissioned the universal voltage divider that was designed and constructed by the JLab detector group in FY16 with funding from this R&D program. The divider allows to vary independently the potential differences between the three PMT stages: cathode–MCP1 (ΔV_1), MCP1–MCP2 (ΔV_2), and MCP2-anode (ΔV_3). For the

studies, we set the overall voltage to −2500 V, ΔV_1=200 V, ΔV_2=2100 V, and ΔV_3=200 V. We took reference data with this voltage distribution at 20° and 0.8 T (where the drop in relative efficiency at standard voltage distribution was observed to be about 60%). Keeping ΔV_2 and ΔV_3 the same, we increased ΔV_1 to 300 V and then to 400 V and measured the PMT response for each setting. Our preliminary results show that: the increase of ΔV_1 by 100 V lead to a gain and efficiency increase by about 15% and 10% respectively, whereas the increase of ΔV_1 by 200 V lead to a gain and efficiency increase by about 23% and 13% respectively. Since the maximum allowed ΔV_1 is 500 V, there is not much room to increase that potential difference for this overall high voltage. This first measurement suggests that the potential difference on the first PMT stage affects both, the gain and the efficiency. The effect on the gain seems to be larger than on the efficiency. The observed efficiency drop at this sensor orientation when B-field increases cannot be significantly compensated by increasing ΔV_1. More detailed studies, in consultation with the manufacturer, for example at other overall HV, should be done in the future in order to study all aspects of this effect.

The studies of backscattering were performed by triggering on the MCP-PMT signal. The discriminator threshold was set to −11 mV (just above the noise level). To increase the probability of observing backscattering signals on the channel that was readout, we removed the mask from the front of the Planacon MCP PMT and illuminated the full area of the sensor. The pulser controlling the LED was operated at 1.65 V, which kept the signal rate at 10% for a HV of −2.5 kV. We counted as backscattering all signals that arrived 20 ns after the end of the primary signal. Figure 3.2.4 shows our preliminary results.

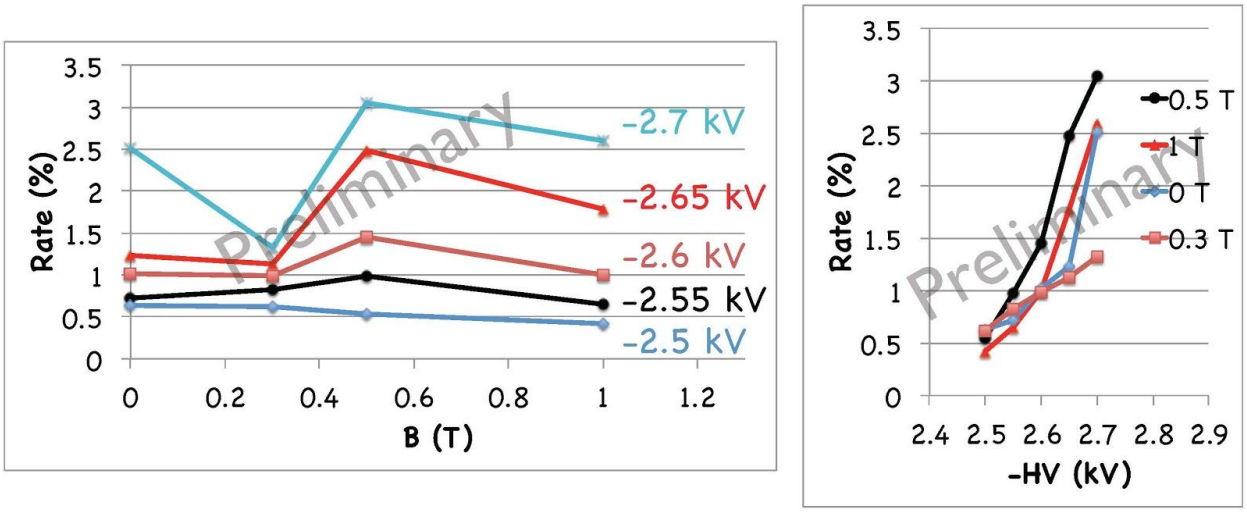

Figure 3.2.4: Estimates of backscattering rate (normalized to number of signals) as a function of B-field magnitude (**left**) and high voltage (**right**) at θ=0°.

Overall, the backscattering seems to be primarily driven by high voltage whereas the field contributes a small amount and only at the highest HV. We are in process of studying the origin of the dips seen on the left figure at B = 0.3 T, where the PMT gain is maximal and of estimating the precision and accuracy of our estimates. For example, the rates seem to be very sensitive to

the value of the minimal amplitude that a waveform should have to be counted as a signal (and not be disregarded as a pedestal).

Note on high voltage and signal amplification: The gain studies we have carried out in the past years aimed to map the **upper limits** of the response of a given MCP-PMT in high B-fields (beyond which the signal amplitude is not viable). For this purpose, both increased HV and variable external amplification were employed. In the past years, we have presented to the committee the gain performance of PMTs at the very upper limit of HV and amplification. For example, for the Planacon 10-μm pore-size sensor, the results at the highest B-fields (2.2 T at θ=0° or 1.5 T at θ=20°) presented last year, were only possible at −2.7 kV and with x20x200 amplification. At a lower HV, no viable signals were observed, independent of external amplification. Ultimately, considerations of PMT lifetime, efficiency, uniform response over a range of relative orientations with respect to the direction of the B-field, *etc.*, that limit the values of the operational parameters will likely lower the B-field for operations below the established upper limits. Thus, the upper limits serve to define the operation-exclusion boundaries in (B, θ) space. Once we understand what the exclusion boundaries are and how they are affected by various parameter changes, we will be able to identify realistic operational parameters.

3.2.2 Future

3.2.2.1 What is planned for the next funding cycle and beyond? How, if at all, is this planning different from the original plan?

For the rest of FY 2019 we plan to (1) perform timing measurements of the 10-μm pore size Planacon MCP PMT as a function of B-field, sensor orientation, and if time permits of high voltage, (2) continue the assessment of PMT efficiency as a function of B-field and sensor orientation, and (3) work on the development of a simulation for optimization of MCP−PMT design parameters as time permits. This plan does not differ from the original plan in terms of content. Due to restricted budget, some of the activities may not be completed in 2019.

Carry-over funds from FY18: USC is carrying over to FY19 $3.4k. JLab is carrying over to FY19 $3k. These funds will be used to procure electronics and components for the timing measurements.

3.2.2.2 What are the critical issues?

The availability of R&D funding at the beginning of the calendar year is critical in order to keep this program within the planned timelines.

3.3 LAPPDs

The LAPPD™ project is a multi-year project involving a number of institutions, with a goal to create an MCP-PMT that has the same very high performance as existing MCP-PMTs, but at a

significantly lower cost. Specifically, for the EIC detector R&D, the effort aims to adapt the LAPPDs to the EIC requirements, which include pixelated readout and acceptable performance in high magnetic fields. With these adaptations, the LAPPDs can be used for the readout of mRICH, dRICH, and DIRC detectors, and for TOF applications.

3.3.1 Past

3.3.1.1 What was planned for this period?

For the period 7/1/18 – 12/31/18, we planned to: (1) produce and test 6 cm MCP-PMT detectors with Incom 10-μm pore size MCPs, the spacing is the same as current standard design; (2) order glass components (side wall and spacer), design and prepare for another 10-μm MCP-PMT with reduced spacing; (3) convince Incom management to devote efforts on delivery of pixelated LAPPD^{TM}; (4) transfer the SLAC MCP-PMT scanning system to ANL, establish 2D single electron efficiency and TTS timing scan capability; (5) enhance MCP-PMT simulation effort to guide MCP-PMT design for high magnetic field.

3.3.1.2 What was achieved?

In FY19, a new MCP-PMT with Incom's ALD functionalized 10-μm pore size MCPs was fabricated by the ANL group. The spacing and side wall used in this MCP-PMT were the same as the standard ones. Detailed configurations of the standard MCP-PMT, this new MCP-PMT without reduced spacing, and the planned next MCP-PMT with reduced spacing are listed in Table 3.3.1.

Table 3.3.1: Detailed configurations of various Argonne 6cm MCP-PMTs

		Standard 20 μm MCP-PMT	**10 μm MCP-PMT without reduced spacing**	**10 μm MCP-PMT with reduced spacing**
MCP	Pore size	20 μm	10 μm	10 μm
	Length to diameter ratio (L/d)	60:1	60:1	60:1
	Thickness	1.2 mm	0.6 mm	0.6 mm
	Open area ratio	60 %	70 %	70 %
	Bias angle	8°	13°	13°
Detector geometry	Window thickness	2.75 mm	2.75 mm	2.75 mm
	Spacing 1	3.25 mm	2.25 mm	2.25 mm
	Spacing 2	1.75 mm	2.0 mm	0.7 mm
	Spacing 3	2.0 mm	4.0 mm	1.1 mm
	Shims	0.3 mm	0.3 mm	0.3 mm
	Tile base thickness	2.75 mm	2.75 mm	2.75 mm
MCP-PMT stack	Internal stack height	**9.70 mm**	**9.75 mm**	**5.55 mm**
	Total stack height	15.20 mm	15.25 mm	11.05 mm

This new MCP-PMT was tested in lab and in magnetic field. The results show a significant improvement of the magnetic-field tolerance and timing resolution. Excellent rise time of 439 ps,

timing distribution root-mean-square (RMS) at single photoelectron mode of 105 ps, timing resolution of 20 ps and magnetic field tolerance up to 1.3 Tesla were achieved for the photodetector with 10-μm pore size MCPs, compared to that of 536 ps, 205 ps, 63 ps and 0.7 Tesla, respectively, for the one with 20-μm pore size MCPs. The results of the 10-μm pore size MCP-PMT are reported in Fig. 3.3.1. The after-pulse signal due to backscattering was significantly suppressed within this tube. The detailed after-pulse performance of this tube was planned to be studied and compared with standard ones to understand the principle of this backscattering suppression.

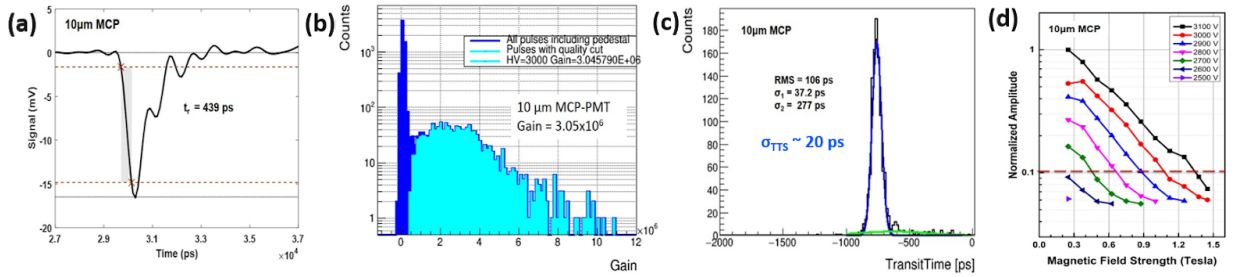

Figure 3.3.1: Characteristics of our new MCP-PMT with 10-μm pore size: (a) waveform with rise time of 439 ps, (b) gain distribution of 3×10^6 with MCPs biased at 1000 V; (c) transit time spread of 20 ps; (d) magnetic field tolerance up to 1.3 Tesla with a signal amplitude reduced to 10% of its value at B=0 T.

Because the spacing reduction will benefit the MCP-PMT magnetic field tolerance and timing resolution, we ordered new components, including side wall, spacer, getter tube and shim for the reduced spacing MCP-PMT fabrication. The components were fully received in late November, and a new 10 μm MCP-PMT with reduced spacing configuration shown in Table 3.3.1 is under fabrication.

Since the last EIC committee meeting and user group meeting in August 2018, the Argonne MCP-PMT group has significantly enhanced the communication and collaboration with Incom, Inc., convincing their management to devote efforts on EIC-PID required LAPPD^{TM}: pixelization and magnetic-field tolerance. The advice and recommendations of the committee as well as feedback from the EIC user group were well explained and emphasized during multiple ANL-Incom bi-weekly meetings, ensuring that the Incom team understands the LAPPD^{TM} requirement for EIC-PID and works towards this direction.

Great progress was also made at Incom, Inc. The first Gen-II LAPPD^{TM} was successfully sealed. Signal pickup through capacitive coupling was demonstrated with 25 mm x 25 mm pixel sizes. Detailed results are presented in Fig. 3.3.2. This success is a great news for the EIC-PID sensor development. Currently, we are negotiating to obtain a prototype Gen-II LAPPD^{TM} at Argonne in Spring or Summer 2019 for EIC-related testing. Since the current Gen-II LAPPD^{TM} capacitive coupling was designed for large pixel sizes, we foresee issues may come out as the pixel size is reduced, especially since EIC-PID requires 3 mm x 3 mm pixel size. Signal pickup, cross talk, timing resolution and other properties may be all different from the standard LAPPD^{TM} ones. Baseline testing of smaller pixel sizes and further development of the signal pickup at 3mm x

3mm through capacitive coupling will require further R&D work. Uniform quantum efficiency (QE) was achieved for a recently fabricated LAPPDs, showing average QE of 24% and a maximum QE of 26%.

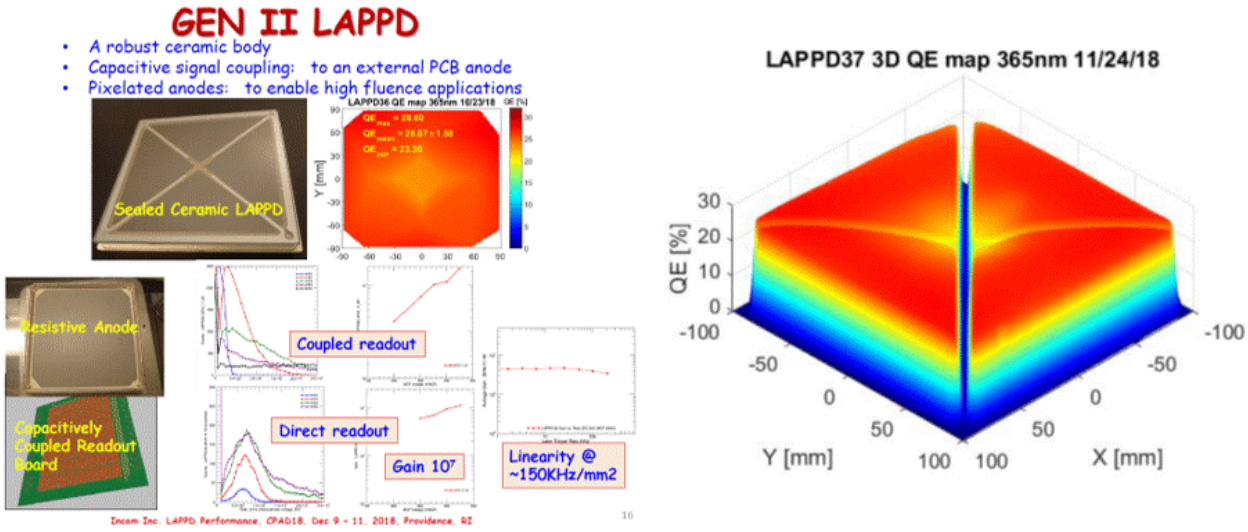

Figure 3.3.2: Left: Prototype Gen II LAPPD^{TM} for pixelated applications, the results were obtained with 25 mm x 25 mm pixel sizes. **Right:** Uniform QE map of a recently manufactured LAPPD, with average QE of 24.26% and maximum QE of 26.05%.

Due to communication and other issues, we were not able to initiate the transfer of the SLAC scanning system to ANL. We are continuing our effort to convince the SLAC team for the system transfer. Meanwhile, we purchased a PiLas 409 nm fast laser, and duplicated the same laser fiber optics system that is used in the JLab High-B facility to establish our capability for single photoelectron efficiency and TTS timing measurement in magnetic fields. A pixelated Photek MAPMT253 (15 μm pore size MCP-PMT with 8x8 pixels) was loaned from Paul Hink at Photek and thoroughly studied at Argonne using this laser system. The magnetic field performance results are reported in Fig. 3.3.3. This measurement provides us the baseline of the Photek pixelated MCP-PMT and directions for future LAPPD^{TM} performance enhancement. Timing resolution was also measured in different B-fields in a SPE mode. The data analysis of the timing resolution dependence on magnetic field magnitude is ongoing.

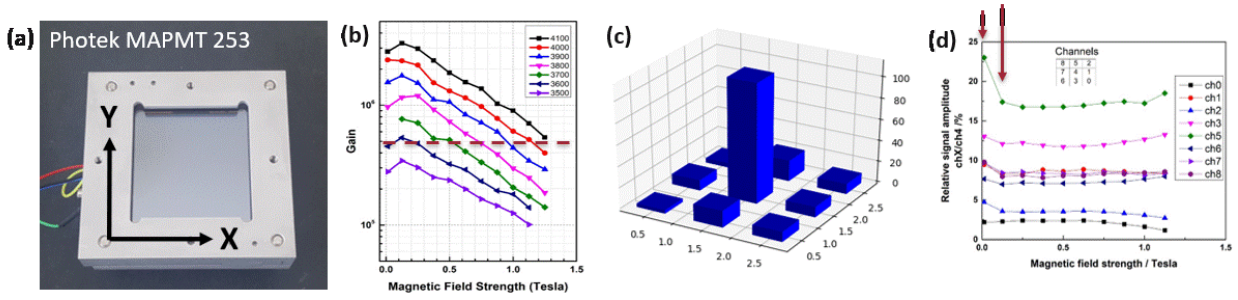

Figure 3.3.3: Magnetic field testing of Photek MAPMT253 with 15-μm pore size and 8x8 pixels: (a) picture of the as-received MAPMT253; (b) magnetic field tolerance up to 1.25 Tesla with gain above 10^5; (c) final electron shower spread (cross talk) with the center pixel illuminated; (d) normalized signal

amplitude dependence on magnetic field, indicating that the signal shower was confined by even a small magnetic field (0.125 T), all the signals after 0.125 T were collected by the center channel, the gain reduction on plot (b) is truly due to the magnetic field.

The MCP-PMT simulation work was successfully initiated at Argonne, we have collaborated with a SIMION software expert to start our simulation work. The work just started in middle of November, more results will be reported later.

The standard LAPPD^{TM} contains Kovar, a magnetic sensitive component, as shims for electric conduction. Under the SBIR program "*Magnetic Field Tolerant Large Area Picosecond Photon Detectors for Particle Identifications*" support, Incom made a design change and replaced Kovar with non-magnetic stainless steel. LAPPD #37 was produced recently, its QE map was shown on the right panel of Fig. 3.3.2. This LAPPD was given to Argonne in early December 2018 for a two-day quick preliminary magnetic field-study, as it needs to be delivered to the ANNIE program to catch up on the experiment's timeline. This magnetic-field preliminary measurement fulfilled the requirement of our SBIR Phase I effort. A Phase II proposal will be submitted in January 2019. For LAPPD #37, the maximum operation HV for MCPs is 850 V. We kept the gap HVs constant ($HV_{photocathode-MCP1}$=100V, $HV_{MCP1-MCP2}$=200V, $HV_{MCP2-anode}$=200V), and varied both MCP bias voltages spontaneously. Figure 3.3.4 shows the preliminary results of this measurement, the signal amplitude decreasing rate of LAPPD #37 is slower than of the 6 cm MCP-PMT, indicating that the LAPPD may have better magnetic field tolerance with the 5 HV bias configuration. Another LAPPD without magnet component is under production and a more comprehensive study on the 5HV bias configuration and the LAPPD performance in magnetic field will be studied.

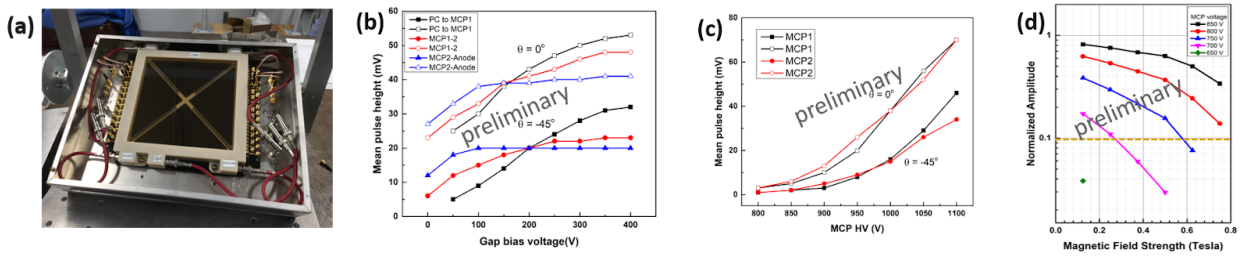

Figure 3.3.4: (a) LAPPD installed with 5 HV configuration; (b) LAPPD performance dependence on the bias voltage applied to each of the three gaps in the LAPPD configuration, the MCP on top, close to photocathode, is labeled as MCP1 while the MCP at the bottom is labeled as MCP2; (c) LAPPD performance dependence on the bias voltage applied to the two MCPs; (d) LAPPD normalized signal amplitude in dependence of magnetic-field strength and MCP bias voltages.

3.3.2 Future

3.3.2.1 What is planned for the next funding cycle and beyond? How, if at all, is this planning different from the original plan?

In the rest of FY19, we plan to continue MCP-PMT fabrication and characterization work as scheduled:

- Fabricate a 10-μm pore size MCP-PMT with reduced spacing
- Explore bias HV effect on the MCP-PMT magnetic-field tolerance
- Establish 2D single electron efficiency and TTS timing scan capability
- Establish MCP-PMT principle simulation with SIMION
- Request prototype Gen-II LAPPD^{TM} from Incom, Inc.
- Explore the pixelated MCP-PMT with small pixel size.
- Test the magnetic-field tolerance of newly produced MCP-PMT and LAPPD^{TM}.

As the committee recommended, MCP-PMT with 5μm pore size is postponed to a later time, after fully understanding of the 10μm pore size MCP-PMTs. More efforts are devoted to the pixelated readout development.

3.3.2.2 What are the critical issues?

Shortness of funding support is continuously the major issue for the ANL MCP-PMT project. The project was previously funded through DOE-HEP detector R&D funding. Since FY17, the Office of HEP at DOE has determined to wind down its support for the LAPPD project. This reduced the funding support for the ANL-LAPPD project by ~1M/year. The optimization of LAPPD MCP-PMTs is now supported by fractional funding from Argonne LDRD, EIC detector R&D, SBIR and HEP base funding to keep the program ongoing at a minimum spending. SBIR phase II proposal will be submitted in January in collaboration with Incom Inc. aiming to understand and further optimize the LAPPD^{TM} design for high-magnetic field tolerance, fast timing LAPPD^{TM} for EIC PID application. Establishing 2D scan capability becomes critical for planned pixel studies as negotiation of Gen-II LAPPD^{TM} delivery at ANL starts.

3.4 Readout Sensors and Electronics for Detector Prototypes

3.4.1 Past

The data acquisition system for the mRICH beam test was provided by the INFN group led by Marco Contalbrigo. There were four Hamamatsu H13700 modules mounted at the sensor plane. The H13700 readout consisted of three circuit boards [Tur15]. The adapter board is a passive board mounting connectors to couple the MA-PMTs socket to the electronics. The ASIC board is based on the MAROC3 chip by OMEGA [Ome18], served by voltage regulators (Analog Devices AD5620). The FPGA board is based on the Xilinx Artix7 and uses the Finisar FTE8510N1LCN optical transceiver to connect to the SSP/VSX DAQ system developed at JLab [Ray14].

The electronics for DIRC beam tests at CERN were mostly provided by the PANDA DIRC group as part of the GSI infrastructure that was made available to the EIC R&D program (although

some compatible items were also procured as part of eRD4 prior to formation of the eRD14 consortium).

3.4.1.1 What was planned for this period?

The development of the readout electronics follows a multi-stage strategy. The goal is to provide a solution for all PID detector R&D needs, and a template for a final system to be used in the full EIC detector. The detailed schedule is adapted to the planned R&D schedule of each system. To experimentally demonstrate the PID performance, the DIRC prototype will eventually have to be instrumented with small-pixel sensors with good timing (<100 ps rms), for which the next-generation SiREAD chip from Nalu Scientific would be ideal. An SiREAD prototype has already been developed through SBIR funding. The new DIRC readout needs to be ready when the prototype is moved to the U.S. (The current tests at CERN use sensors and electronics available at GSI.) The initial priority is thus to develop a readout for the RICH detectors, and in particular the mRICH, which had carried out its second beam test in the first half of 2018. The similarity between the sensors considered for the dRICH and mRICH also allows the latter to serve as a (sensor and readout) prototype for the former. It is our hope that even if the detailed requirements of the two systems would eventually diverge somewhat, a high degree of commonality can be retained. We also plan to use SiREAD for the next iteration of the readout for the RICH detectors – allowing for further synergies.

The primary goal for this reporting period was the development of a readout firmware for an upcoming mRICH beam test, which will follow the very successful mRICH beam tests at Fermilab in April 2016 and June 2018. A goal of this next beam test is to fully verify the PID capability by using the same photosensors, which utilize finer pixel size (3mm x 3mm) from Hamamatsu: H13700A multi-anode PMTs and cooled MPPC (SiPM) arrays. For this test, there is no requirement for <100 ps timing (which the CLAS12 electronics cannot fulfill). The availability of the two readout prototypes allow for direct comparison of the performance. One prototype will again use a readout based on an evolution of the tested CLAS12 electronics provided by the INFN group (M. Contalbrigo) and one based on the sampling electronics from the U. Hawaii group (G. Varner) and Nalu Scientific, LLC (I. Mostafanezhad). The latter was initially based on the TARGETX chip, used in the electronics provided by that group for the Belle II upgrade at KEK. However the longer-term goal has been to switch over to the new SiREAD chip, the experience gained with an intermediate version based on TARGETX, as well as the cross reference with the CLAS12 electronics, will be an important part of the R&D process. The 64-channel SiREAD chip (32ch prototype) is currently being developed by Nalu Scientific, a small business specializing in System-on-Chip data acquisition systems, which has recently been awarded multiple DOE Phase I and Phase II SBIRs to develop the next generation readout electronics for HEP/NP applications. The goal is to have the readout electronics (both INFN/CLAS12 and Hawaii/TARGETX) ready for test in late spring 2019.

3.4.1.2 What was achieved?

U. Hawaii (G. Varner) has partnered with Nalu Scientific to develop a readout solution for mRICH using new readout ASICs. The SiREAD chip was fabricated and tested at Nalu Scientific through funding from the DOE SBIR program. While SiREAD chip was in fabrication, a rev 1.0 PCB level design has been developed using the existing TARGETX chip. Such a design allows to rapidly test the electronic performance of readout scheme when coupled with the MCP-PMT or SiPM array. Figure 3.4.1 shows a photo of the fabricated 256-channel TARGETX based readout coupled with the H13700 PMT and a rendering of the expanded version to read out 1024 channels for the 2019 beam test. If there is a decision to move to a SiPM array, the design is inherently flexible enough to allow such migration with minimal amount of redesign. Figure 3.4.2 shows the fabricated 32-channel prototype SiREAD chip with 1 GSa/s digitization and System-on-Chip digital processing capabilities. The SiREAD was connected to a SiPM element and dark counts were recorded on a testbench.

In parallel, the INFN group worked on upgrading the readout electronics (based on the JLab CLAS12 RICH electronics) for reading out the high channel density H13700 modules and explored the option for using SiPM array with cooling. The progress is on track. This may allow us to test both photosensors during the next mRICH beam test.

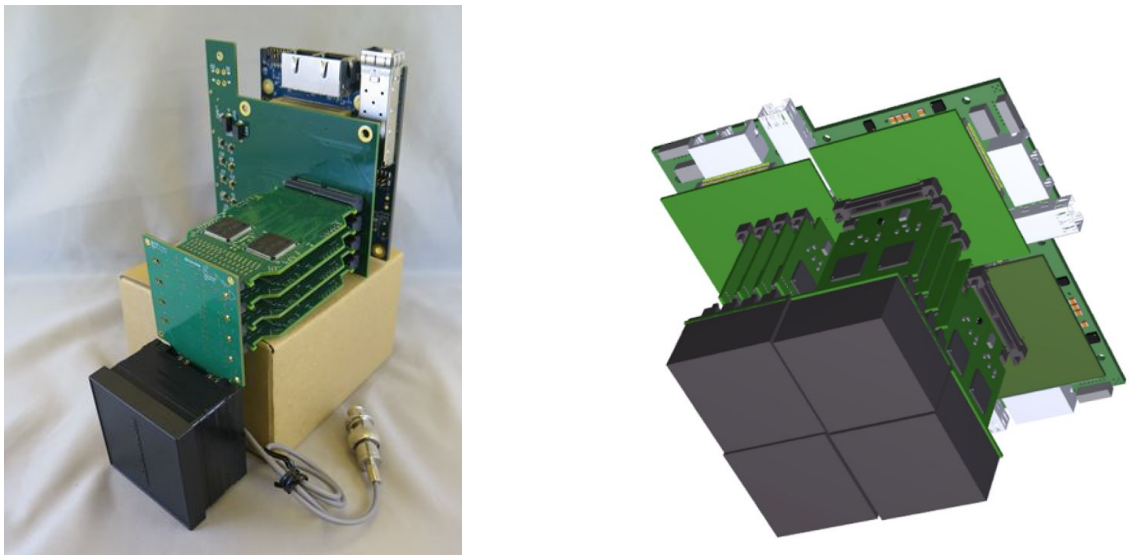

(a) **(b)**

Figure 3.4.1: 3D rendering of the readout electronics proposed for H13700 PMT. (a) fabricated single PMT readout for 256 channels, and (b) rendering of four modules abutted to read out 1024 channels.

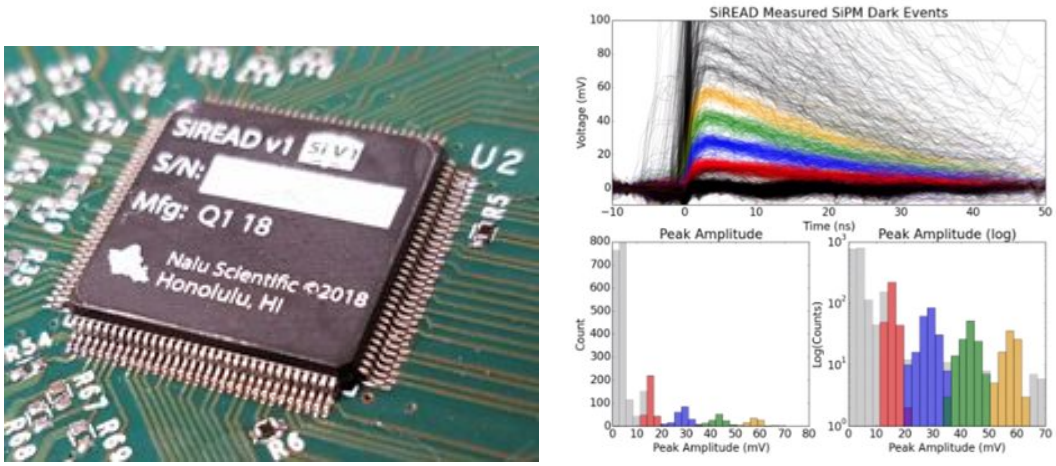

(a) **(b)**

Figure 3.4.2: (a) Fabricated prototype 32-channel SiREAD chip. (b) Dark count measurements on a SiPM using the SiREAD chip showing 1pe, 2pe,... waveforms and histograms.

3.4.2 Future

3.4.2.1 What is planned for the next funding cycle and beyond? How, if at all, is this planning different from the original plan?

The consortium is developing readout electronics for future R&D needs. The plan is on track and will result in a system that can satisfy the needs of all the Cherenkov detectors (DIRC, dRICH, mRICH). The first version will be supplied for the next mRICH beam test at Fermilab, likely in the first half of 2019. Given capabilities of the prototype SiREAD, we will develop and adapt readout boards to connect the MCP-PMT to SiREAD for a more efficient readout scheme.

References:

[Tur15]
http://infn.fe.infn.it/~mcontalb/JLAB12/RICH_midterm_review/RICH_Electronics_Turisini.pdf

[Ome18]
http://omega.in2p3.fr/index.php/download-center/doc_details/393-proceedingsieeenss2010maroc3.html

[Ray14]
https://coda.jlab.org/drupal/system/files/pdfs/HardwareManual/SSP/SSP_Module_HallD_v1.2.pdf

4. Manpower

Abilene Christian University

Rusty Towell, Faculty

Argonne National Laboratory

Junqi Xie, Staff Scientist, 75% of time spent on project

Bob Wagner, Staff Scientist, 20% of time spent on project

Lei Xia, Staff Scientist, 20% of time spent on project

Edward May, Argonne Associate, 50% of time spent on project

Frank Cao, Student, 20% of time spent on project

Tim Cundiff, Electronics Engineer, 5% of time spent on project

Frank Skrzecz, Mechanical Engineer, 5% of time spent on project

Brookhaven National Laboratory

Mickey Chiu, Staff Scientist

Andrey Sukhanov, Electronics Engineer

Rob Pisani, Scientific Associate

Catholic University of America

Grzegorz Kalicy, Faculty, 50% of research time on project

Duke University

Zhiwen Zhao, Research professor

Georgia State University

Xiaochun He, Faculty, 20% of time spent on project.

Xu Sun, new postdoc, 50% of time on the project, supervised by X. He.

William Roh, graduate student, 30% of time on this project, supervised by X. He

GSI Helmholtzzentrum für Schwerionenforschung

Roman Dzhygadlo, Staff Scientist, 25% of time spent on project

Carsten Schwarz, Staff Scientist, 15% of time spent on project

Jochen Schwiening, Senior Staff Scientist, 15% of time spent on project

Howard University

Marcus Alfred, Faculty, 25% of time spent on project

INFN

Marco Contalbrigo, researcher, 10% of time spent on project

Evaristo Cisbani, researcher, 10% of time spent on project

Vincenzo Lucherini, researcher, 10% of time spent on project

Marco Mirazita, researcher, 10% of time spent on project

Luca Barion, post-doc, 40% of time spent on project supervised by M. Contalbrigo

Jefferson Lab

Carl Zorn, Staff Scientist

Los Alamos

Hubert van Hecke, Staff Scientist (ret.)

Old Dominion University

Charles Hyde, Faculty, 30% of research time on project

Stony Brook University

Pawel Nadel-Turonski, Adjunct Professor, 30% of research time spent on project

University of Hawaii

Gary Varner, Faculty, 10% of time spent on project

Tommy Lam, Undergraduate Student, 100% of time until departed for Virginia Tech to attend graduate school, supervised by G. Varner

Emily Lum, Undergraduate Student, 50% time, supervised by G. Varner

Nathan Park, Undergraduate Student, 50% time, supervised by G. Varner

University of Illinois at Urbana-Champaign

Matthias Grosse-Perdekamp, Faculty

University of South Carolina

Yordanka Ilieva, Faculty, 30% of time spent on project

Alan Rowland, Undergraduate Student, 17% of time spent on project (8 weeks), located at Jefferson Lab, supervised by Y. Ilieva, C. Zorn, and J. McKisson

Andrew Dunton, Undergraduate Student, 5% of time spent on project (2 weeks), located at Jefferson Lab, supervised by Y. Ilieva

Colin Gleason, Postdoctoral Fellow, 5% of time spent on project (2 weeks), located at Jefferson Lab, supervised by Y. Ilieva

Tongtong Cao, Postdoctoral Fellow, 5% of time spent on project (2 weeks), located at Jefferson Lab, supervised by Y. Ilieva

Include a list of the existing manpower and what approximate fraction each has spent on the

project. If students and/or postdocs were funded through the R&D, please state where they were located and who supervised their work.

5. External Funding

ANL

- ANL-LDRD project: A Strategic Scientific Program to establish Argonne Leadership in the Development of the Future Electron-Ion Collider, Oct 1, 2018 – Sep 30, 2019: $70k
- SBIR project: Magnetic Field Tolerant Large Area Picosecond Photon Detectors for Particle Identifications, Apr 9, 2018 – Jan 9, 2019: $50k
- DOE-HEP detector R&D (KA25) base funding

ODU

- University funds for fast (picosecond) laser pulser procurement for High-B timing measurements: $15k.
- University funds for travel for CERN PS test beam, Oct 10 - Nov 3, 2016: $4k.
- DOE Grant funding for Graduate Research Assistant, 100% on project: $19,000 (including indirect costs), 1 July 2016 — 31 December 2017

GSU

- University funds provided the major portion of the support for a graduate student and the research staff. We also used the university funds for purchasing building materials of constructing the mRICH prototypes and the supporting frames.

GSI

- Mechanical and monitoring component replacement for DIRC prototype in preparation of transfer to US in FY20: $12k.
- Spherical lens prototype (non-radiation hard) test production: $13k.
- Travel for DIRC prototype beam test at CERN PS, Jul 26 - Aug 15, 2018: $18k.
- GSI travel funds for the annual DIRC@EIC meeting: $7k.

UHawaii

- DOE Detector R&D (Hawaii Grant Task F) support for new detector development and ASIC training stewardship, roughly $100k annually, 25% spent this reporting period..

INFN

- dRICH: prototype mechanics, procurement of gas and aerogel for tests; mRICH+dRICH: SiPM and cooling system; electronics; travel expenses: EU 12 k.

BNL

- Infrastructure and staff salary for the radiation hardness tests of DIRC and mRICH optical materials.

Jefferson Lab

- Salary of staff (detector experts, DAQ, electronics, technicians), facilities, equipment, and infrastructure for the High-B MCP-PMT evaluations.
- Conference space for the annual DIRC collaboration meeting, phone conferencing for the bi-weekly consortium meetings and any other consortium-related remote meetings.

See also the respective sections for more details on TOF, photosensors, etc.

6. Publications

6.1 In Preparation

A. Del Dotto et al., *Event based inverse ray-tracing reconstruction for RICH detector*, to be published in NIM (likely first half of 2019).

6.2 Recently Published or Submitted

X. He (EIC PID Consortium), *RICH Detector Development for the Electron Ion Collider*, submitted to NIM A, under review.

Junqi Xie, Marcel Demarteau, Edward May, Robert Wagner, and Lei Xia, *Fast-timing microchannel plate photodetectors: design, fabrication and characterization*, Review of Scientific Instruments, (Submitted, under review, 2018).

Junqi Xie, Klaus Attenkofer, Marcel Demarteau, Alexander Paramonov, Anatoly Ronzhin, Robert Wagner, and Zikri Yusof, *Large Area Planar Photocathode for MCP-based Photodetectors*, Nuclear Instruments and Methods in Physics Research Section A, (Submitted, under review, 2018).

Mohammad Hattawy, Junqi Xie, Mickey Chiu, Marcel Demarteau, Kawtar Hafidi, Edward May, Jose Repond, Robert Wagner, Lei Xia, and Carl Zorn, *Characteristics of fast timing MCP-PMTs in magnetic fields*, Nuclear Instruments and Methods in Physics Research Section A, (Submitted, under review, 2018).

Junqi Xie, Mohammad Hattawy, Mickey Chiu, Kawtar Hafidi, Edward May, Jose Repond, Robert Wagner, and Lei Xia, *Rate capability and magnetic field tolerance measurements of fast timing microchannel plate photodetectors*, Nuclear Instruments and Methods in Physics Research Section A, 912 (2018) 85. https://doi.org/10.1016/j.nima.2017.10.059

7. Presentations

A. Rowland (EIC PID Consortium), *Studies of MCP-PMT Gain in High Magnetic Fields*, poster presentation at the Conference Experience for Undergraduates at the 5th Joint Meeting of the APS Division of Nuclear Physics and the Physical Society of Japan, 23 – 27 October, Waikoloa, HI, 2018.

A. Rowland (EIC PID Consortium), *Studies of MCP-PMT Gain in High Magnetic Fields*, poster presentation at The 85th annual meeting of the APS Southeastern Section, 8 – 10 November, Knoxville, TN, 2018.

X. He (EIC PID Consortium), *RICH Detector Development for the Electron Ion Collider*, invited talk, 10th International Workshop on Ring Image Cherenkov Detectors, Moscow, Russia, July 29 – August 4, 2018.

X. Sun, *Modular Ring Imaging Cherenkov Detector for Particle Identification in the Electron-Ion Collider (EIC) Experiments*, RICH & AGS Annual Users' Meeting, Brookhaven National Laboratory, Upton, NY, June 12 – 15, 2018.

G. Kalicy, *Update of R&D for the High-Performance DIRC for the Future Electron Ion Collider Experimen*t, Physics Colloquium at the CUA University, Washington DC, August 29th, 2018.

G. Kalicy, *The High-Performance DIRC Detector for the Future Electron Ion Collider Experimen*t, 2018 IEEE Nuclear Science Symposium and Medical Imaging Conference, Sydney, Australia, November 10 – 17, 2018.

J. Xie, *Development of MCP-PMT/LAPPD towards EIC application*, Electron Ion Collider Users Group meeting, Washington, DC, August, 2018.

J. Xie, *Fast-timing microchannel plate photodetectors: design, fabrication and characterization*, 5th International Workshop on New Photon-Detectors (PD18), Tokyo, Japan, November 27 – 29, 2018.

J. Xie, *Development of Fast-timing MCP-PMT/LAPPD™ for Particle IDentification (PID)*, CPAD

Instrumentation Frontier Workshop 2018, Providence, RI, December, 2018.